Synthesis and characterization of ferrocenyl bearing transition metal dithiocarbamate complexes [M{κ^2*S,S*-$S_2CN(CH_2R)CH_2Fc$}$_n$]: Thermogravimetric, cyclic voltammetric, fluorescence and antimicrobial study

Abstract

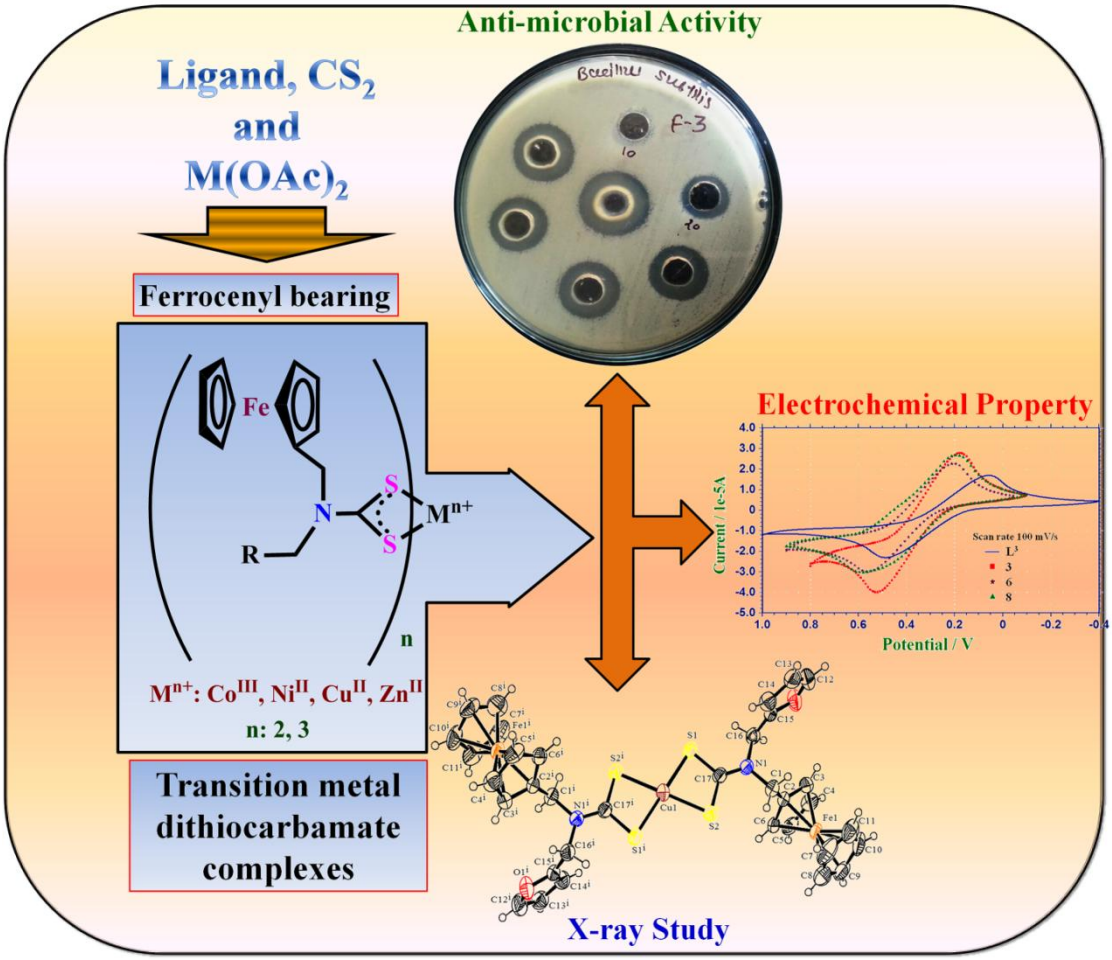

A facile single pot reaction involving self-assembly of *N*-methyl-(1-naphthyl)-*N*-methylferrocenyl amine (L^1), *N*-methyl-(3-pyridyl)-*N*-methylferrocenyl amine (L^2) or *N*-furfuryl-*N*-methylferrocenyl amine (L^3) with CS_2 and $M(OAc)_2$ in Et_3N, affords access to a series of ferrocenyl bearing transition metal dithiocarbamate complexes of the type [M{κ^2*S,S*-$S_2CN(CH_2R)CH_2Fc$}$_n$] {M = Co^{III}, R = 1-naphthyl, (**1**), 3-pyridyl (**2**), 2-furyl (**3**); M = Ni^{II}, R = 1-naphthyl, (**4**), 3-pyridyl (**5**), 2-furyl (**6**); M = Cu^{II}, R = 1-naphthyl, (**7**), 2-furyl (**8**); M = Zn^{II}, R = R = 1-naphthyl, (**9**); n = 3 for **1-3** and n = 2 for **4-9**}. All the new compounds were thoroughly characterized by microanalysis and

standard spectroscopic methods such as MS, IR, ^{1}H, ^{13}C, DEPT 135 NMR, UV-vis. absorption and emission spectroscopy. Single crystal X-ray diffraction technique was used to detect new polymorphic form of **8**. It is of significance to realize that cooperative S/lp···π and C–H...π interactions play an important role in crystal packing of **8**. $\mathbf{L^1}$-$\mathbf{L^3}$ and **1**-**9** were screened against a panel of bacteria: *Staphylococus aureus, Bacillus subtilis*, *Escherichia coli, Pseudomonas aeruginosa* and fungi: *Candida albicans*, *Aspergillus niger*. Interestingly, $\mathbf{L^1}$, **4** and **8** exhibits enhanced antibacterial activity against *Staphylococus aureus* and proved to be more potent than *Ciprofloxacin*. While **5** emerges as a better antifungal agents against *Candida albicans* than the reference drug *Flucanazole*. The TGA/DTA analysis reveals that the amine precursors decomposes spontaneously to form metallic iron. All the complexes display a single quasi-reversible cyclic voltammograms due to the dominant redox-active ferrocenyl moieties and formal redox potentials in the range of 407 to 224 mV vs. Ag/Ag+ (CH_3CN).

2.1. Introduction

Since the inception of ferrocene [1] there is a substantial growth in the chemistry utilizing the ferrocene [2,3] as a foundation stone in terms of the design and synthesis of new compounds, typically because of its lipophilic character, ease of chemical modification and accessible one-electron-oxidation potential. In spite of its nontoxic nature, stability in aqueous and aerobic media, biological inertness, many ferrocenyl derivatives exhibit significant anticancer, antibacterial, antiparasitic, antifungal, and other biological activities and thus appeared at the forefront of bioorganometallic chemistry [4]. The biological activity of such derivatives is reportedly associated with the attachment of the ferrocenyl group to either biologically relevant molecules or with the molecules that do not exhibit biological activity on their own. Potential examples include ferrocenyl analogues of tamoxifen [5] and the antiparasite ferroquine derivatives [6] where ferrocenyl fragment efficiently potentiate the biological activity of the conjugated pharmacophore. Edward's research group have synthesized a series of antibiotics containing ferrocene moiety such as ferrocenyl penicillin, ferrocenyl cephalosporine and ferrocenyl hybrid of penicillin and cephalosporine [7].

On the other hand, metal complexes with sulfur-rich ligands are very interesting from the viewpoint of their electrical conductivity, molecular magnetism, electrochemistry, optoelectronic properties and biological processes [8,9]. In particular, dithiocarbamate have drawn a lot of attention since its first derivative tetramethylthiuram disulfide, more commonly known as thiram has achieved prominence fungicidal properties [10]. Compounds having dithiocarbamate (DTC) group, were proven medicinally significant and utilized as microbicidal spermicides, [11] anesthetic, [12] anti-HIV, [13] mono glyceride lipase inhibitors, [14] anti-tumour agents [15]. The unique redox properties of the sulfur atom in DTC make it a key residue for enzyme catalysis, protein folding, and redox signaling and regulation, [16] which are important for cellular energy metabolism, motility and subsistence of cellular systems. The above properties of the DTC group make it a versatile pharmacophore and hence, it is used in the compounds of biological interest.

In the light of unprecedented increase of multidrug resistance in common pathogens and the rapid emergence of new infections, [17] development of new antimicrobial agents is more urgently needed than ever. The major causes of fatal nosocomial infections as well as community-acquired infections are Staphylococcus aureus (S. aureus, Gram-positive bacteria) and Pseudomonas aeruginosa (P. aeruginosa, Gram-negative bacteria) [18]. The spread of these organisms in healthcare settings is often difficult to control due to the presence of multiple intrinsic and acquired mechanisms of antimicrobial resistance. Moreover, the most prominent fungal pathogens affecting human being are Candida albicans, which remains the predominant cause of invasive candidiasis [19].

Although, there are a few reports on the transition/non-transition metal DTC complexes screened for fungal toxicity in in vitro conditions [20]. To the best of our knowledge, this is the first report on the anti-microbial activity of ferrocenyl incorporated DTC complexes of transition metals ever published. Since, the incorporation of ferrocenyl moieties into the structures of the existing drug molecules has demonstrated an important strategy to increase their therapeutic properties, we anticipate that the combination of the ferrocenyl group with biologically relevance pharmacophore DTC could be a successful method to discover a new promising antimicrobial candidate of different physicochemical properties.

2.2. Results and discussion

2.2.1. Synthesis and characterization

The ferrocene bearing secondary amines *N*-methyl-(1-naphthyl)-*N*-methylferrocenyl amine (L^1), *N*-methyl-(3-pyridyl)-*N*-methylferrocenyl amine (L^2) or *N*-furfuryl-*N*-methylferrocenyl amine (L^3) were synthesized following a modified literature procedure [3a] (Scheme 1) and these were fully characterized, prior to use. Distinctly, the reaction of ferrocenyl methanamine ($FcCH_2NH_2$) with 1-naphthaldehyde in refluxing toluene yielded required imine for the synthesis of $\mathbf{L^1}$, using Dean–Stark apparatus (Scheme 1). Dean–Stark apparatus facilitate the condensation of amines and various aldehydes [21] by removing H_2O, formed during the progress of the reaction; it shifts the equilibrium towards the product with higher yield and in less time.

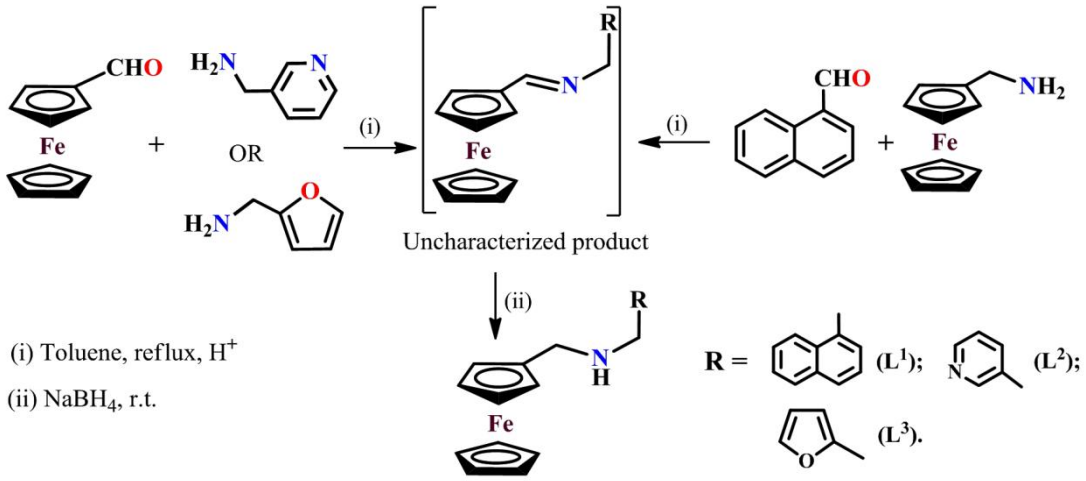

Scheme 1. Preparation of ferrocenyl bearing amine precursors $\mathbf{L^1}$, $\mathbf{L^2}$ and $\mathbf{L^3}$.

Interestingly, a single pot reaction involving self-assembling of L^1, L^2 or L^3 with CS_2 and $M(OAc)_2$ in Et_3N affords access to a series of ferrocenyl bearing transition metal dithiocarabamte complexes of the type $[M\{\kappa^2S,S\text{-}S_2CN(CH_2R)CH_2Fc\}_n]$ {M = Co^{III}, R = 1-naphthyl, (**1**), 3-pyridyl (**2**), 2-furyl (**3**); M = Ni^{II}, R = 1-naphthyl, (**4**), 3-pyridyl (**5**), 2-furyl (**6**); M = Cu^{II}, R = 1-naphthyl, (**7**), 2-furyl (**8**); M = Zn^{II}, R = R = 1-naphthyl, (**9**); n = 3 for **1-3** and n = 2 for **4-9**} in good yield (Scheme 2). Complexes **6** (Ni) and **8** (Cu) are reproduced [3b] by improved procedure (scalable up to > 90 % yield) to investigate and compare the anti-microbial property with a number of analogous compounds. All compounds are fairly soluble in common organic solvents and found to be stable in solid state and in the solution over a period of days. Though, a majority of compounds could not be obtained in crystalline form, their compositions and structures were established satisfactorily by

microanalysis and standard spectroscopy. The ESI-/ LC-MS (CH_3CN) of all complexes **1-9** gave molecular ion peaks (m/z) which either corresponds $[M]^+$ or $[M+H]^+$ along with differential fragmentation peaks (supplementary information) and

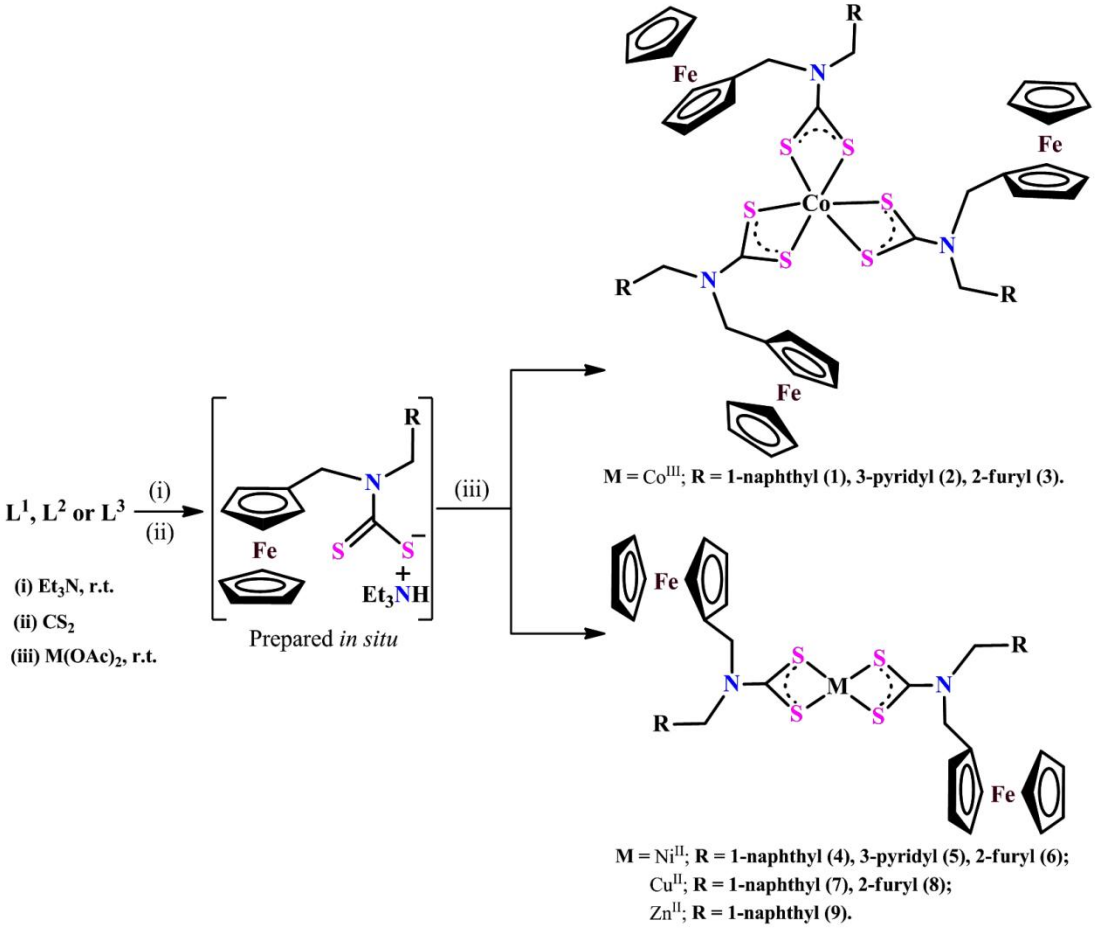

Scheme 2. Synthesis of ferrocenyl bearing transition metal dithiocarbamate complexes **1-9**.

thus confirmed the formation of corresponding complexes. The characteristic IR bands for $\mathbf{L^1}$-$\mathbf{L^3}$ and complexes **1-9** are summarized in the experimental section. As expected, the υ(N-H) band (3200-3350 cm^{-1}) seen for amine precursor $\mathbf{L^1}$–$\mathbf{L^3}$ (supporting information) is disappeared from the corresponding IR spectrum of **1-9** and two new single sharp medium intensity bands are appeared in the 1460-1494 cm^{-1} and 991-1027 cm^{-1} regions, attributable to ν(N-CS_2) and ν(C-S) stretching frequencies, associated with the symmetric bidentate dithiocarbamate lignads [22]. Further, NMR study confirms the purity and composition of $\mathbf{L^1}$–$\mathbf{L^3}$ as well as diamagnetic complexes. The NMR data are summarized in the experimental section. The ^{1}H NMR spectrum of the ligand precursors $\mathbf{L^1}$, $\mathbf{L^2}$ or $\mathbf{L^3}$ displays characteristic –NH proton signal at δ 3.25, 2,24 and δ 2.4 ppm, which is obviously absent in the ^{1}H

NMR spectrum of the corresponding complexes. The assignments of ^{1}H and ^{13}C NMR were supported by corresponding DEPT 135 study. ^{1}H and ^{13}C NMR spectra of these compounds corroborate the presence of methylene, aryl and ferrocenyl groups. A careful comparison of the ^{1}H NMR spectra (supporting information) of the complexes with corresponding amine precursors, it appears that all complexes experience significant down-field shifting of signals related to methylene hydrogen atoms associated with NCH_2Ar/ NCH_2Fc- substituents (**2**: $\Delta\delta$ = 0.83/0.92, **3**: $\Delta\delta$ = 0.72/0.91, **4**: $\Delta\delta$ = 0.68/0.41, **5**: $\Delta\delta$ = 0.72/0.82, **6**: $\Delta\delta$ = 0.63/0.81, **9**: $\Delta\delta$ = 1.28/0.92). This noticeable shifting of signals is due to the presence of dithiocarbamate moiety in the complexes. Additionally, the ^{13}C NMR spectrum of **9** exhibits a very downfield signal at 207 ppm, a characteristic feature of coordinated dithiocarbamate (-CS_2) moiety derived from secondary amine precursors [23] and thereby confirms the formation of dithiocarbamato complexes.

2.2.2. UV-Visible absorption and magnetic moment study

The electronic emission spectral data of $\mathbf{L^1}$-$\mathbf{L^3}$ and complexes **1-9** recorded in 10^{-5} M DMSO solution is given in [Table 1] The electronic absorption spectrum of $\mathbf{L^1}$-$\mathbf{L^3}$ gives single sharp band in 268-283 nm region (Fig. 1, Fig. 2 and Fig. 3) which is mainly attributed to the locally excited intra-ligand $\pi\rightarrow\pi^*$ transitions [24]. All the complexes apparently display a high intensity band in the 259-274 nm region, attributable to the $\pi\rightarrow\pi^*$ intra-ligand transition along with a medium intensity band in 323-438 nm regions which can be assigned to the ligand to metal (LMCT) charge transfer transitions, characteristic of coordinated dithiocarbamate (-NCS_2) ligands [25]. Expectedly, Co(III) **1-3** and Cu(II) **7-8** complexes display a low intensity broad band in the 620-655 nm regions [26]. The μ_{eff} = 1.87 and 1.86 BM (BM: Bohr magneton) of copper complexes **7** and **8** specify the existence of one unpaired electron on the Cu(II) centre. The cobalt and nickel complexes are diamagnetic indicating the formation of a low-spin Co(III) $3d^6$ and Ni(II) d^8 complexes, respectively. The magnetic moment values (Table 1) along with UV-visible absorption bands suggest an octahedral environment around Co(III), the square planar environment around Ni(II)/ Cu(II) and tetrahedral environment around Zn(II) centres in their respective dithiocarbamate complexes [27].

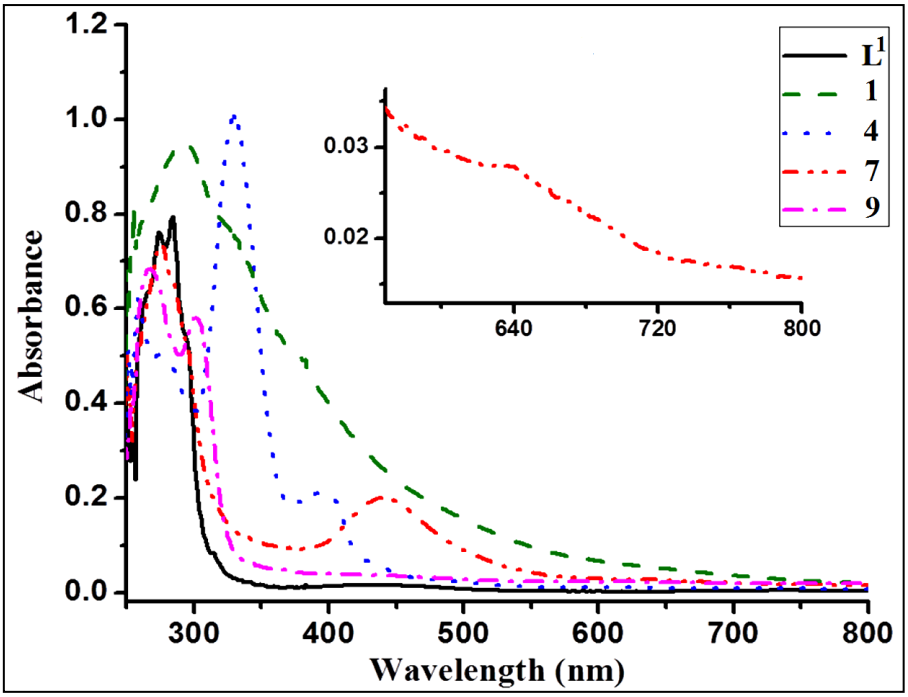

Fig. 1. UV-visible absorption spectra of the ligand precursor ($\mathbf{L^1}$), its dithiocarbamate complexes **1, 4, 7** and **9** at room temperature in 10^{-5} M DMF solution.

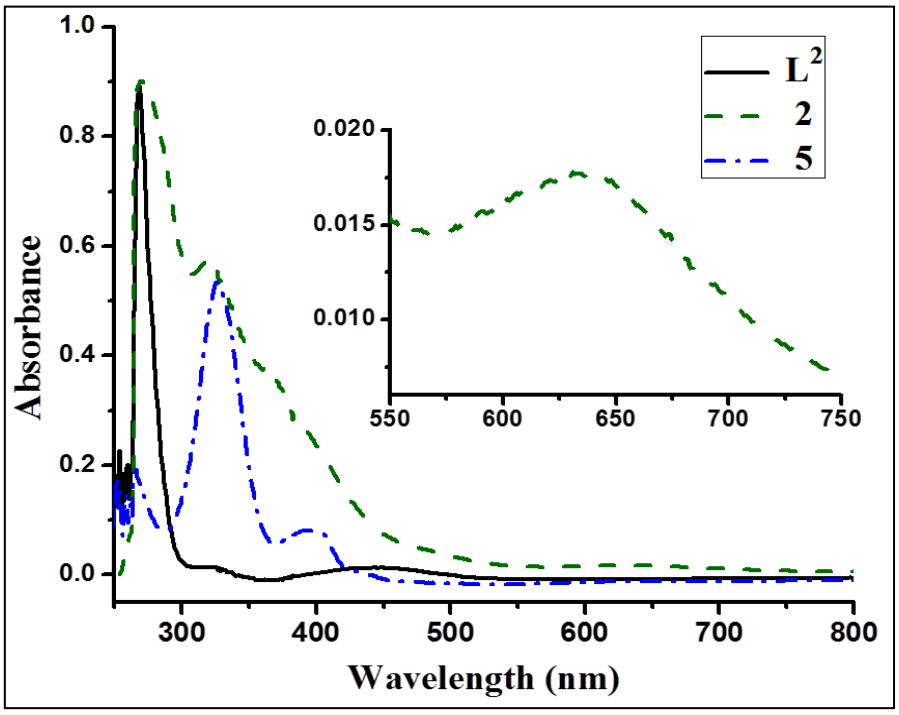

Fig. 2. UV-visible absorption spectra of the Ligand precursor (L^2), dithiocarbamate metal complexes 2 and 5 at room temperature in 10^{-5} M DMF solution

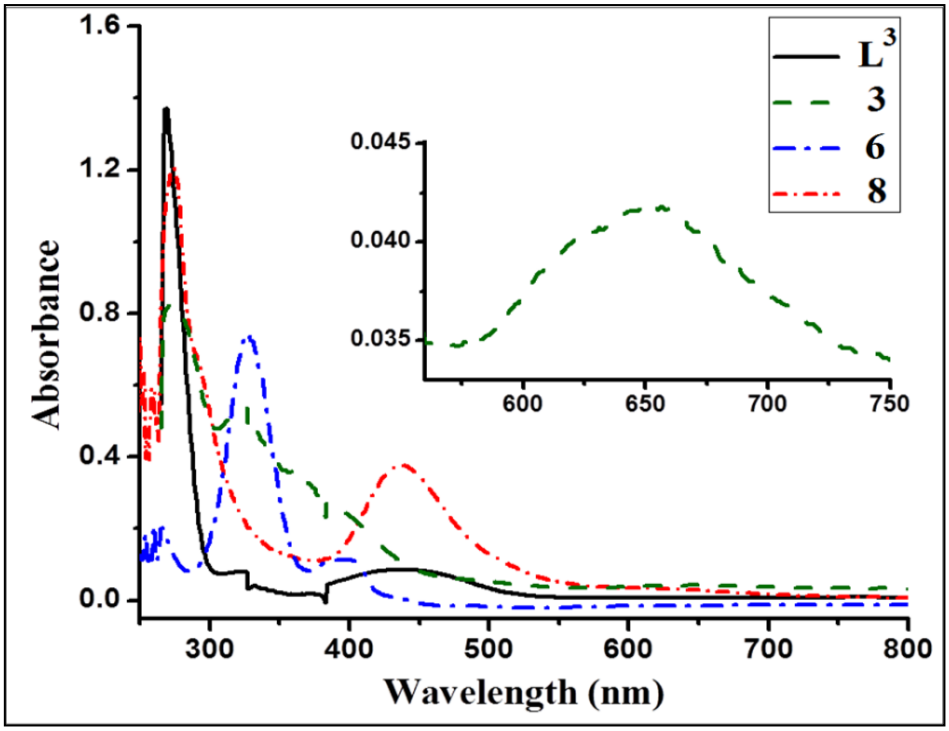

Fig. 3. UV-visible absorption spectra of the Ligand precursor (L^3), dithiocarbamate metal complexes 3,7 and 8 at room temperature in 10^{-5} M DMF solution

Table 1
UV-visible and fluorescence spectral data of ligand precursors and complexes 10^{-5} M in DMF

Entry	λ_{max} nm (10^{-5} M, ε L $Mol^{-1}cm^{-1}$)	Magnetic Moment μ_{eff}(BM)	Fluorescence spectral data (10^{-5} M DMF)	
			λ_{ex} nm	λ_{em} (nm) (Intensity)
L^1	283(79375) π→π*	-	283	338 (77) π*→π
L^2	268(89081) π→π*	-	268	Non fluorescent
L^3	268(137231) π→π*	-	268	342 (35) π*→π
1	292(95076) br , π→π*, 333 (73092) n→π*	dia	292	341 (4.5) π*→π
2	270(90355) π→π*, 323(57714) n→π*, 636(01774) *d-d* transition	dia	270	469 (58), 486 (55) π*→π
3	273(82411) π→π*, 325(54159) n→π*, 655(04176) *d-d transition*	dia	273	353 (11), 460 (13) π*→π
4	259(61977) π→π*, 328(101441) n→π*, 397(21239) charge transfer	dia	259	Non Fluorescent
5	267 (19200) π→π*, 329(53150) n→π*, 395(07910) charge transfer	dia	329	Non fluorescent
6	265 (20058) π→π*, 326(74291) n→π*, 394(11356) charge transfer	dia	326	Non fluorescent
7	274(74348) π→π*, 438(20391) charge transfer, 639(2813) d-d transition	1.87	274	Non Fluorescent
8	274(120599) π→π*, 437(37648) charge transfer, 624(3310) d-d transition	1.86	274	342 (32) π*→π
9	267(68081) π→π*, 299 (58027) n→π*	dia	267	349 (88), 467 (41) π*→ π

2.2.3. Fluorescence emission study

The fluorescence emission data of the ligand precursors **L^1, L^2, L^3** and complexes **1-9** is summarized in Table 1. **L^1** and **L^3** fluoresces at 338 and 342 nm upon excitation at λ_{ex} = 283 and 268 nm but **L^2** did not exhibit any noticeable fluorescence emission. Among all the complexes, Zn(II) complex **9** exhibits maximum fluorescence emissions (Fig. 4), essentially at two wavelengths 349, 467 nm with concomitant Stokes shifts of 82, 200 nm, when excited at higher energy band 267 nm. As expected, the Ni(II) complexes **4-6** and Cu(II) complex **7** are appeared to be non fluorescent; these do not exhibit any fluorescence emission band upon excitation of either higher energy or lower energy bands because of their well known quenching behavior. However Co(III) **2** and Cu(II) complex **8** fluoresce noticeably at 469/486 and 342 nm upon excitation at λ_{ex} = 270 and 274 nm, respectively with significant Stokes shifts. A very weak fluorescence emission was observed for other Co(III) complexes **1** and **3**. The observed trend of fluorescence spectra and concomitant bathochromic shifts of intramolecular charge-transfer emissions is consistent with earlier reports [28]. The emergence of a number of bands upon excitation of a single wavelength as well as high fluorescence behaviour of the Zn(II) complex **9** may be attributed to the reduction of photoinduced electron transfer process on complex formation [29]. Literature evidences dependency of the fluorescence properties of the compounds on the molecular arrangements, achieved by means of polymorphism, conformational stiffness of the fluorophore (dihedral angles), non-covalent interactions such as π…π or C-H…π and on the nature of substituents which can principally affect the photoinduced electron transfer processes [30].

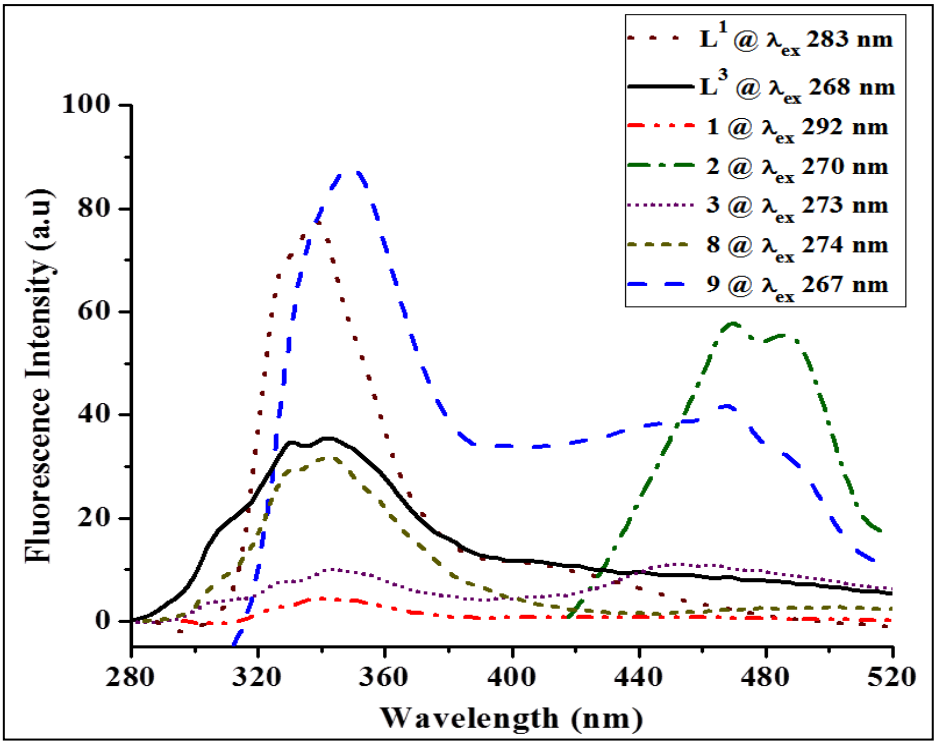

Fig. 4. Fluorescence emission spectra of the ligand precursors ($\mathbf{L^1}$, $\mathbf{L^3}$) and mononuclear dithiocarbamate complexes **1-3**, **8-9** at room temperature in 10^{-5} M DMF solution.

2.2.4. Single Crystal X-ray Crystallography

For crystals of compound **8**, the intensity data were collected at 293(2) K on a Nonius Kappa CCD diffractometer system equipped with graphite-monochromated CuKa radiation (λ=1.5418Å). The structures were solved by direct methods (SIR97) and refined by a full-matrix least-squares procedure based on F^2. All non-hydrogen atoms were refined anisotropically; hydrogen atoms were located at calculated positions and refined by using a riding model with isotropic thermal parameters fixed at 1.2 times the Ueq value of the appropriate carrier atom.

2.2.5. Crystal structure determination and packing patterns

Many drugs reportedly received regulatory approval only for a single crystal form or polymorph because of the dependency of important physico-chemical properties on the exact crystal form of a polymorph. This highlights the importance of polymorphism in the development of pharmaceutical ingredients [31]. Due to differences in solubility of polymorphs, one polymorph may be more active therapeutically than another polymorph of the same drug. The synthetic and analytic

departments of leading pharmaceutical companies nowadays carry out systematic work to detect polymorphism of their drugs, [32] since the discovery of the first cases of polymorphism with dramatic differences in biological activity between two forms of the same drug *i.e.* chloramphenicol palmitate. The statement that the substance exhibits no polymorphism is equally important as exhibiting polymorphism.

Single crystals of **8** were grown in DMF and studied by means of single crystal X-ray diffraction technique. Unlike the earlier structure, [3b] compound **8** crystallizes in a monoclinic $P2_1/c$ space group. The X-ray crystal structure of this shows a half of the molecule of $[C_{17}H_{16}Cu_{0.5}FeNOS_2]$ in its asymmetric unit and a complete molecule is generated through symmetry operation is shown in Fig. 5a. There are four such units present in the unit cell. The relevant parameters are tabulated in Table 2. These values were found in the normal range (vide supra). The copper centre of **8** has adopted the square-planar geometry by the coordination of four sulphur atoms of the metalloligand N-furfuryl-N-methylferrocenyl dithiocarbamate. The Cu1–S1 and Cu1–S2 bond lengths are 2.2845(12) Å and 2.2972(11) Å respectively. The bite angle S1–Cu1–S2 is 77.63(4)° respectively. The two chelate rings involving Cu1, S1, S2 and C17 atoms are coplanar. The N1–C17 bond length for **8** (1.318(5) Å) is intermediate to those of the C–N (1.47 Å) and C=N (1.28 Å) bonds and indicate the partial double-bond character between the N1–C17 bonds in the complex.

Table 2. Crystal data, structure refinement, bond angles (º) and bond length (Å) for **8**.

Identification code	**8**		
Empirical formula	$C_{17}H_{16}Cu_{0.5}FeNOS_2$	**Bond Angles (deg)**	
Formula weight	402.07	N1-C17-S2	123.6(3)
Temperature (K)	293	N1-C17-S1	123.0(3)
Wavelength (Å)	1.5418	S2-C17-S1	113.4(2)
Crystal system	monoclinic	$S2^i$-Cu1-S2	180.0
space group	$P2_1/c$	S2-Cu1-S1	77.63(4)
Unit cell dimensions(Å/ °)	a = 7.68390(18)	S1- Cu1-$S1^i$	180.0
	b = 10.8592(3)	S2-Cu1-$S1^i$	102.37(4)
	c = 20.2399(5)	C17-S2-Cu1	84.49(14)
	α = 90	C17-S1-Cu1	84.48(14)
	β = 93.150(2)	**Bond length (Å)**	
	γ = 90	C17-N1	1.318(5)
Volume/$Å^3$	1686.29(7)	C17-S2	1.709(4)
Z	4	C17-S1	1.727(4)
Calculated density/Mg/m^3	1.5836	Cu1-S2	2.297(11)
Absorption coefficient/ m/mm^{-1}	10.126	Cu1-S1	2.2845(12)
F(000)	817.9	C1-N1	1. 474(5)
Crystal size/mm^3	0.1 × 0.08 × 0.07	C16-N1	1.463(5)
Theta range for data collection	8.76 to 143.92°		

Limiting indices	$-6 \leq h \leq 9$, $-13 \leq k \leq 12$, $-23 \leq l \leq 24$
Reflections collected	5061
Independent reflections	3186[R(int) = 0.0253]
Goodness-of-fit on F^2	1.054
Final R indices [I>2sigma(I)]	$R_1 = 0.0502$, $wR_2 = 0.1477$
Largest diff. peak and hole/ e $Å^{-3}$	0.64 and -0.55

Of more fascinating, the single crystal X-ray diffraction data: space group, cell volume and crystal packing patterns, clearly demonstrate the formation of a polymorphic form [3b] of **8** in DMF. Particularly, crystal packing patterns of reported polymorph of **8** is predominantly stabilized by C-H...S donor-acceptor interactions only that involve Cp rings of ferrocene and S atoms of the coordinated dithicarbamate moieties. However, the molecules of **8** have shown the propensity of formation an emerging S/lp...π contacts in cooperation with C-H...π intermolecular contacts as shown in Fig. 5b. S/lp...Cg1(Centroid: O1C12C13C14C15) interactions lead to 1D stacking interaction in **8**, arranging the molecules along a-axis (Fig. 5c). The S/lp...Cg1 and S/lp...C14(Cg1) distances of 4.198 Å and 3.452 Å, respectively, are appearing in the normal range [33a] Recently, the lp···π intermolecular interaction has become significantly important in supramolecular chemistry [33] and biology [34]. The energies of these interactions appeared in the range of −4 kcal mol^{-1} to −12 kcal mol^{-1} depending on the availability of the lp of electrons on an oxygen/sulfur atom. Apart from this interaction, both the Cp rings of each ferrocene units of **8** are primarily involved in C-H...π donor-acceptor interactions, respectively, connecting the molecules in *bc*-plane through C3-H3...Cg2 (Centroid: C7C8C9C10C11) contacts, forming an attractive 2D sheet that possesses a number of openings (cavity size ~6.9 × 11.2 $Å^2$) as shown in Fig. 5d. The protocols for this interaction, *i.e.* distances C3-H3...Cg2 (3.029 Å), C3...Cg2 (3.765 Å), ∠C3-H3-Cg2 (β =137.21º) and the angle between the vector along the Cg2–H line and the normal to the plane of the ring (C7C8C9C10C11) (α = 21.47º) are consistent with the earlier reports [3b,24b]. The mutual effect of these interactions assembled the molecules of 8, forming a 3D infinite network as shown in Fig. 5e.

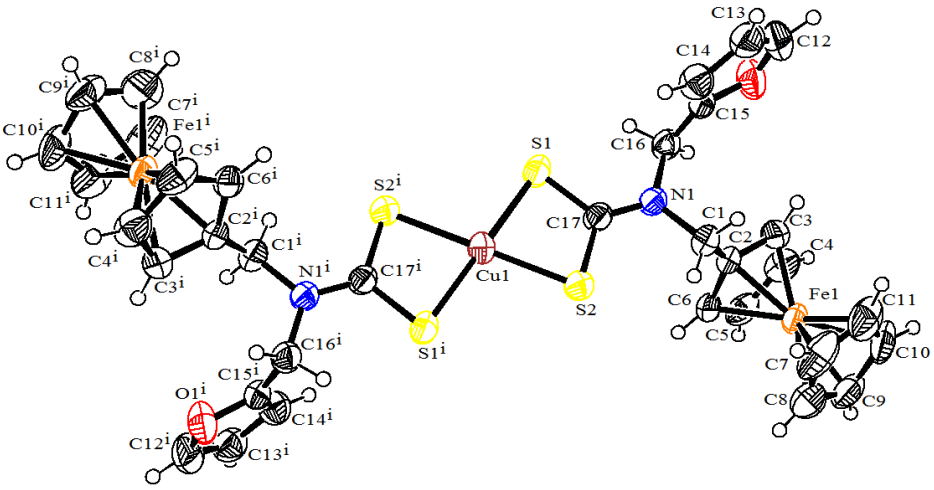
C13
C12
C14
C15
C16
S1
N1
C1
C2
C3
C4
C17
S2i
Cu1
S2
C6
Fe1
C11
C5
C7
C10
C8
C9
C8i
C9i
C7i
Fe1i
C10i
C5i
C6i
C11i
C2i
C1i
C4i
N1i
C3i
C17i
S1i
C16i
C15i
O1i
C14i
C12i
C13i

(a)

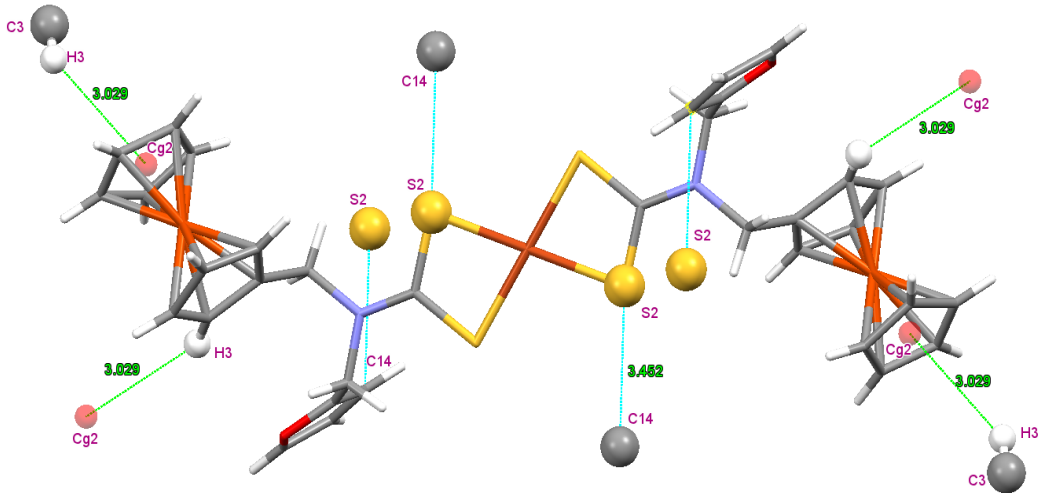
C3
H3
3.029
Cg2
C14
S2
S2
S2
S2
3.029
Cg2
H3
3.029
Cg2
C14
3.452
C14
Cg2
3.029
H3
C3

(b)

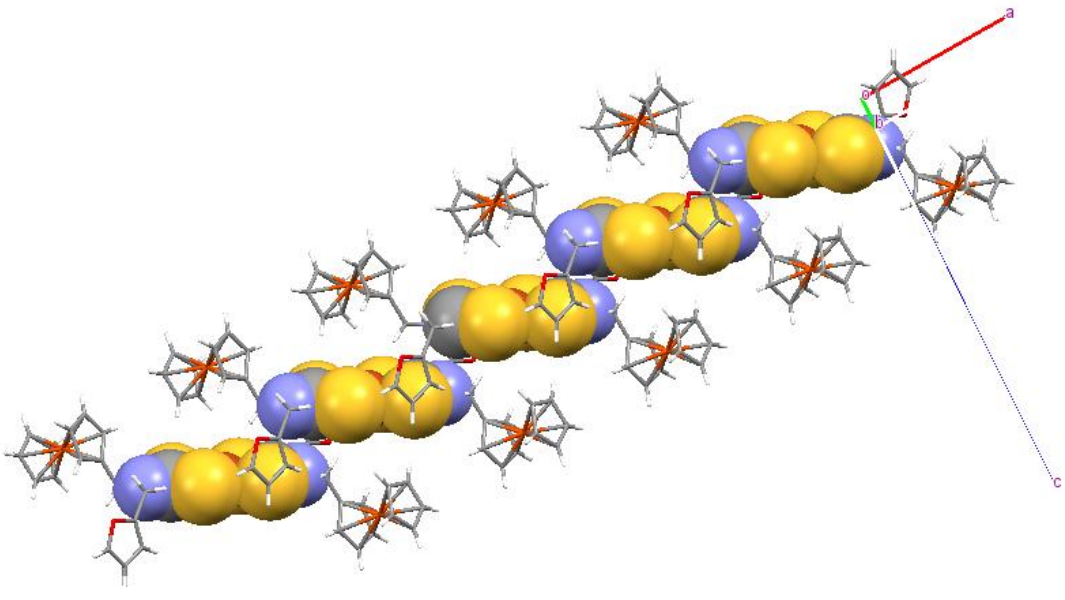
a
c

(c)

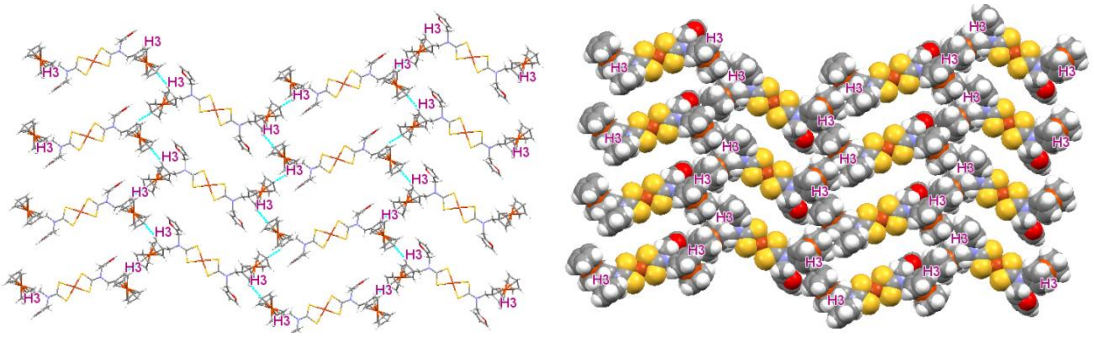

Capped Stick representation **Spacefill representation**

(d)

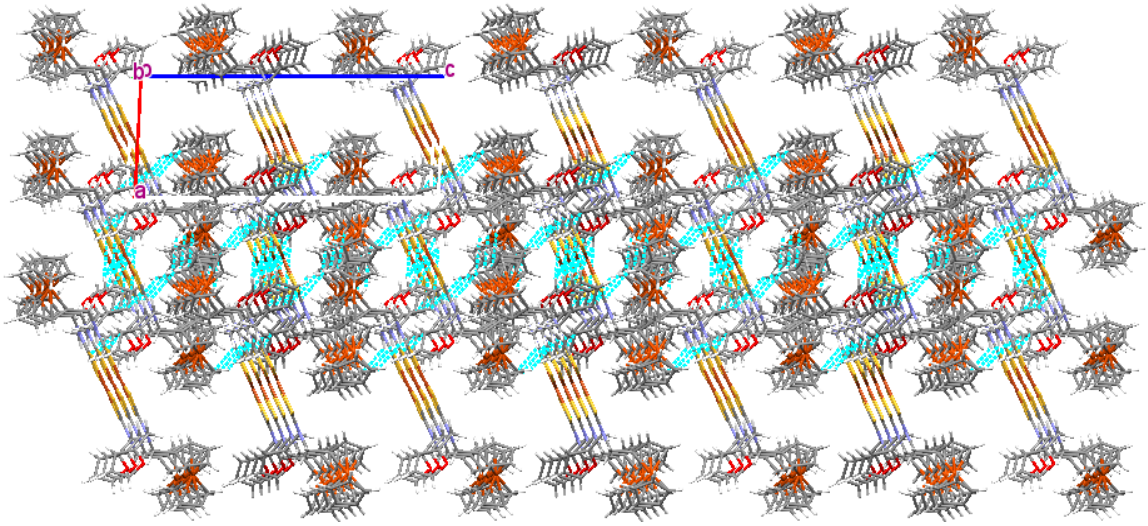

(e)

Fig. 5. (a) The ORTEP view of compound **8** at 50% probability; (b) Propensity of formation of S/lp...π contacts in cooperation with C-H...π intermolecular interaction in molecules of **8**; (c) Stacking interaction involving S/lp....π interactions along a-axis; (d) Capped Stick and Spacefill representation of molecular packing through C-H...π interactions in bc-plane; (e) 3D molecular packing of **8** involving C-H...π and S/lp...π interactions, view along the b-axis with 3×3×3 packing.

2.2.6. Electrochemical study

A large part of the biological activity of ferrocenyl bearing organic and organometallic compounds is shown to be related to their electron-transfer ability [35]. Thus, it becomes pertinent to investigate the electrochemical behaviour of these newly synthesized compounds. The oxidation potential and peak current of one-electron ferrocene/ferrocenium redox couple in ferrocenyl bearing compounds can be

efficiently tuned by the variation of substituents at the cyclopentadienyl ring that can be exploited for the estimation of useful electrochemical parameters and substituent effect.

The electrochemical behaviour of the ligand precursors $\mathbf{L^1}$-$\mathbf{L^3}$ and ferrocenyl bearing transition metal dithiocarbamate complexes **1-9** were investigated at potential scan rate of 100 mVs^{-1} by cyclic voltammetry. Before experiments, the dissolved oxygen gas was removed from the solution with purged nitrogen gas. Voltammograms were recorded by using anhydrous solutions of these compounds in CH_2Cl_2 containing $^{n}Bu_4NPF_6$ (0.1M) as supporting electrolyte. The oxidation (E_{pa}) and reduction (E_{pc}) peak potentials along with the peak potential separation (ΔEp) and the formal redox potentials (E^o) are summarized in Table 3. Initial electrochemical examination of $\mathbf{L^1}$-$\mathbf{L^3}$ clearly demonstrates only one quasi reversible oxidation wave with the formal redox potentials at E^o = 407, 298.5 and 271.5 mV, respectively (Fig. 6, Fig. 7 and Fig. 8). It appears that the redox potential of $\mathbf{L^1}$ bearing *N*-1-naphthylmethyl substituent is largely shifted anodically, compared to $\mathbf{L^2}$-$\mathbf{L^3}$ and their dithiocarbamate complexes. This large shift of the redox potential of $\mathbf{L^1}$ at a higher potential side showed its superior electrochemical efficiencies, which is further reflected by its enhanced anti-microbial properties, discussed later. Similar to the earlier reports, [3a,b] the voltammograms of all the ferrocenyl bearing transition metal dithiocarbamate complexes examined in this work, did not display any additional peak and the complexes are primarily electro active with respect to the dominant redox-active ferroceyl moieties. The redox active transition metal cations in the dithiocarbamate complexes are thus present in silent mode. Further, electrochemically equivalence of poly ferrocenyl units in all the complexes is confirmed by emergence of a single quasi-reversible wave. When compared the electrochemical responses of the complexes with corresponding ligand precursors $\mathbf{L^1}$-$\mathbf{L^3}$, complexes **3**, **6** and **8** exhibit redox potentials that are significantly shifted anodically, however the redox potentials of the rest of the complexes are shifted cathodically. Complexes derived from $\mathbf{L^1}$ and $\mathbf{L^3}$ display higher efficiency than a number of previously reported [3a,b] ferrocenyl bearing transition metal dithiocarbamate complexes. In general, the electrochemical response of Ni(II) complex **6** is found to be higher than Cu(II) complex **8** which is consistent with the literature reports [3b]. Zn(II) complex **9** bearings *N*-(1-naphthylmethyl) substituents, contrarily exhibit superior efficiencies than analogues Cd(II) complexes bearing *N*-benzyl substituent, [3a] revealed by

advanced shifting of redox potential at a higher potential side. A density functional theory (DFT) calculations, performed on the ferrocenyl bearing transition metal dithiocarbamate complexes, suggest that the electron is mainly released from the Fe during the oxidation. The spin density surface plots for the 1e- oxidized species further highlight the delocalization of positive charge around Fe atom. The results reveal that the formal potential varies in the sequence $\mathbf{L^3}$<$\mathbf{L^2}$<$\mathbf{L^1}$, suggesting the idea that the electrochemical oxidation behavior of the oxidizing moiety ferrocene can be modulated by changing the electronic properties of the substituents near to the cyclopentadienyl ring. The strong electron-withdrawing 1-naphthyl makes the oxidation of the iron in $\mathbf{L^1}$ difficult by significant anodic shifting the oxidation potential.

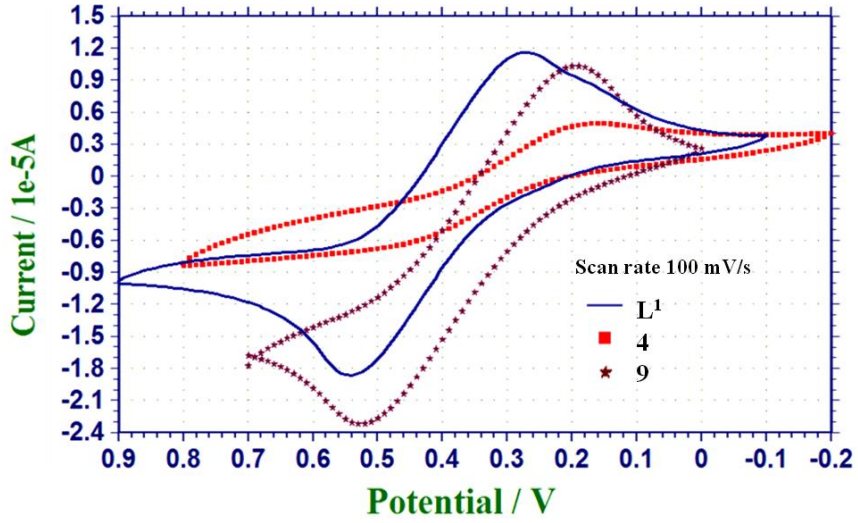

Fig. 6. Cyclic voltammograms of a 1.0 mM solution of the ligand $\mathbf{L^1}$ and its dithiocarbamate metal complexes **4** and **9** in dichloromethane containing 0.1 M tetra-n-butylammonium hexafluorophosphate as the supporting electrolyte.

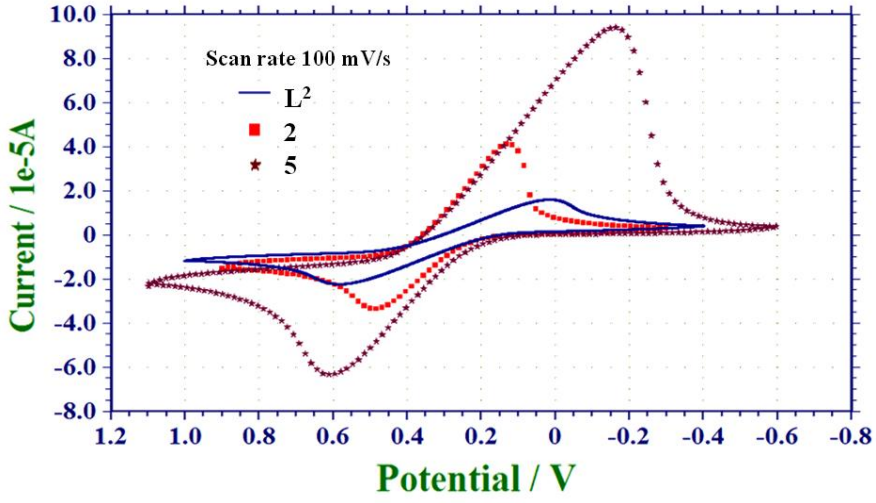

Fig. 7. Cyclic voltammograms of a 1.0 mM solution of the ligand $\mathbf{L^2}$ and its dithiocarbamate metal complexes **2** and **5** in dichloromethane containing 0.1 M tetra-n-butylammonium hexafluorophosphate as the supporting electrolyte.

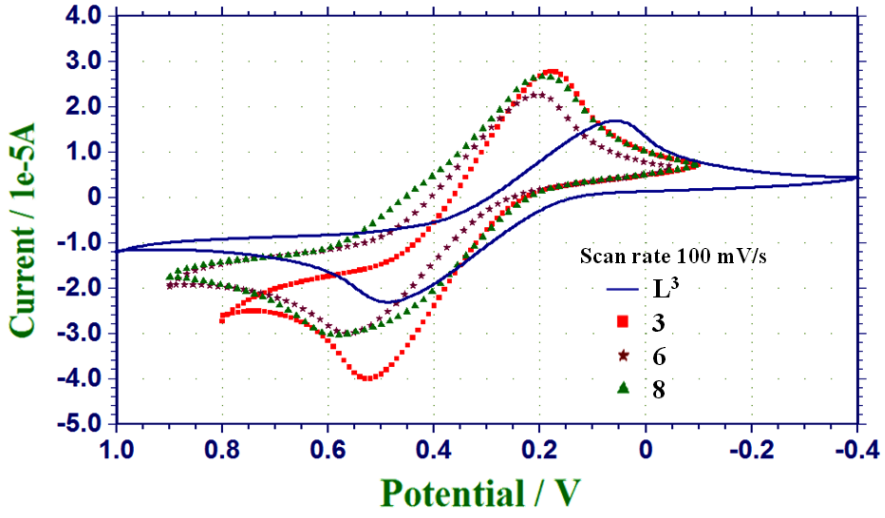

Fig. 8. Cyclic voltammograms of a 1.0 mM solution of the ligand $\mathbf{L^3}$ and its dithiocarbamate metal complexes **3, 6** and **8** in dichloromethane containing 0.1 M tetra-n-butylammonium hexafluorophosphate as the supporting electrolyte.

Table 3
Electrochemical data for the compounds $\mathbf{L^1}$-$\mathbf{L^3}$ and ferrocenyl bearing dithiocarbamate complexes obtained at a scan rate of 100 mVs^{-1}.

Entry	$E_{p,c}$ (mV)	$E_{p,a}$ (mV)	$\Delta Ep = E_{p,a} - E_{p,c}$ (mV)	$E^o = (E_{p,a} + E_{p,c})/2$ (mV)
L^1	271	543	272	407
L^2	14	583	569	298.5
L^3	57	486	429	271.5
2	127	487	360	307
3	177	525	348	351
4	162	515	353	338.5
5	-162	610	772	224
6	206	562	356	384
8	182	576	394	379
9	192	526	334	359

2.2.7. Thermogravimetric Analysis

Thermal properties of the ligand precursors $\mathbf{L^2}$, $\mathbf{L^3}$ and complexes **1-9** were studied in the temperature ranges from room temperature to 750 ºC. Heating rate was suitably guarded at 10º C min^{-1} under nitrogen atmosphere. The differential weight losses over a range of temperature, rate of thermal decomposition and the residual masses

corresponding to final degradation products are summarized in [Table 4]. A single or multi stages of mass loss for these compounds were observed with DTG and corresponding DTA peaks, attributed to endothermic and/or exothermic elimination of molecular fragments due to the thermal degradation. The thermogravimetric plots (Supporting Information, Fig. S30) of $\mathbf{L^2}$ and $\mathbf{L^3}$ clearly evidences a sharp endothermic peak on DTA curves at 50.4 and 45.8 ºC respectively, without any significant mass loss on DTG curves, due to the phase change that can be assigned to the melting points of these compounds. The TG curves clearly demonstrate that $\mathbf{L^2}$ and $\mathbf{L^3}$ decomposed completely with a maximum rate of decompositions (0.972 mg min^{-1} for L^2 and 0.252.3 mg min^{-1} for L^3) recorded at 298.4, 252.3 °C respectively, on DTG curves. The stable residual masses of 18.3 and 16.2 for $\mathbf{L^2}$ and $\mathbf{L^3}$ correspond to Fe (calc. 18.2 and 18.9 %, respectively). The formation of Fe nanoparticles during thermogravimetric analysis of ferrocenylethynylbenzenes has been previously [36]. Further reports suggest that at temperatures above ~770K, gaseous ferrocene decomposes spontaneously to form metallic iron via evolution of H_2, CH_4 and other organic volatiles [37]. Notably, the thermal decompositions of all the complexes **1-9** starts before their melting points and accompanied by the appearance of one or more endothermic peak on corresponding DTA curves. It appears that the complexes bearing N-(1-naphthylmetyl)- substituents **1**, **4**, **7** and **9** are thermally unstable as their decompositions start at a lower temperature (100-160 ºC), compared to other complexes which are indeed stable up to 200 ºC. The degradation of **2**, **5**, **7** and **8** is essentially taking place in single stage while three stages of degradations are observed on TG curved for other complexes. The three stages of degradation of complex **9** involves the losses of Cp groups in the first stage, losses of naphthyl groups in the second stage and the evolution of CS_2 in third stage. This can be clearly seen from the residual mass obtained on TG curve (Fig. S30, Table 4). Similarly, the formation of expected degradation products for **1-9** in different temperature ranges is summarized in Supporting Information (Table 4). In contrast to our earlier reports, [22b,28a,38] the thermal degradation of the ferrocenyl bearing transition metal dithiocarbamate complexes **1-9** could not lead to the formation of either corresponding metal sulphides or metal sulphates.

Table 4. Thermogravimetric data of the ligands $\mathbf{L^2}$, $\mathbf{L^3}$ and dithiocarbamate metal complexes **1–9**.

Entry	Steps	Temp. range (°C)	Weight loss on TG (%)	DTA peak (°C)	DTG peak (°C)	Rate of decomposition (mg min^{-1})	Residue (%) Found (Calcd.)	Final product
$\mathbf{L^2}$	I	180-500	81.7	50.4	--	--	18.3	
				269.4	229.0	0.459	(18.2)	Fe
				288.2	298.4	0.972		
				478.4	439.4	0.416		
$\mathbf{L^3}$	I	190-350	83.8	45.8	252.3	0.792	16.2	Fe
				255.6	296.2	0.670	(18.9)	
				300.2	324.4	0.329		
1	I	120-150	18.7	--	128.0	0.073	49.1	
	II	151-350	18.1	--	250.4	0.047		-
	III	351-740	14.1	--	523.1	0.024		
2	I	200-740	49.4	259.1	261.5	0.567	50.6	-
3	I	230-190	1.9	232.4	231.6	0.572	76.9	-
	II	191-350	17.5					
	III	351-690	3.7					
4	I	110-220	2.8				65.1	-
	II	221-430	29.3	243.3	247.6	0.799		
	III	431-680	2.8					
5	I	250-730	54.5	246.7	255.9	0.678	45.5	-
				258.3	270.9	0.454		
6	I	200-210	1.0	204.1	197.3	0.033	69.1	-
	II	211-320	23.6		222.3	0.447		
	III	321-700	6.3					
7	I	160-650	44.0	203.7	201.3	0.192	56.0	-
8	I	200-650	36.9	201.7	204.0	0.264	63.1	-
9	I	100-150	24.5	102.2	102.6	0.737	38.6	-
	II	151-310	29.2	255.6	282.4	0.324		
	III	311-550	7.7					

2.2.8. Biological study

The stability of the ferrocenyl group in non-aqueous, aqueous, aerobic media, the accessibility of a large variety of derivatives, and its favorable electrochemical properties make ferrocene and its derivatives very popular molecules for biological applications.[4-8] A literature review suggests that the biological action of these compounds is attributed to the presence of ferrocenyl moieties that increases the cell permeability, lipophilicity, action of metabolites towards biomolecues [39].

$\mathbf{L^1}$–$\mathbf{L^3}$ and **1-9** were screened by Broth dilution method [40] for their antibacterial activity against two gram positive bacteria S. aureus and B. subtilis, two

gram negative bacteria E. coli and P. aeruginosa. They were also evaluated for their in vitro antifungal activity against C. albicans and A. niger. Concentration of compounds was ranged from 10µg to 600µg/ml. It was ascertained that the solvent had no antibacterial or antifungal activities against any of the test microorganisms. Ciprofloxacin and Flucanazole were used as standard drugs also tested under the similar conditions for comparison. The minimum inhibitory concentration (MIC) of the synthesized compounds that prevented visible growth are given in Table 5. Among $\mathbf{L^1}$–$\mathbf{L^3}$, the activity of $\mathbf{L^1}$ is found to be excellent against S. aureus (MIC = 10 $\mu g ml^{-1}$) and very good against B. subtilis (MIC = 20 $\mu g ml^{-1}$) gram positive bacteria, however, this showed poor activity against both of the investigated gram negative bacteria (Fig. 9). Further, $\mathbf{L^2}$ displayed a good activity against S. aureus and E. coli and a moderate against P. aeruginosa while $\mathbf{L^3}$ showed moderate activity only against S. aureus and poor against other bacteria. The ferrocenyl bearing dithiocarbamate complexes derived from $\mathbf{L^1}$ exhibits moderate to excellent activity against all the tested bacteria. For instance, Ni(II) **4** and Cu(II) **7** complexes are appeared to be excellent and very good anti-bacterial agents, respectively, against gram positive bacteria S. aureus whereas other complexes exhibit moderate to good activity against both of the investigated bacteria.

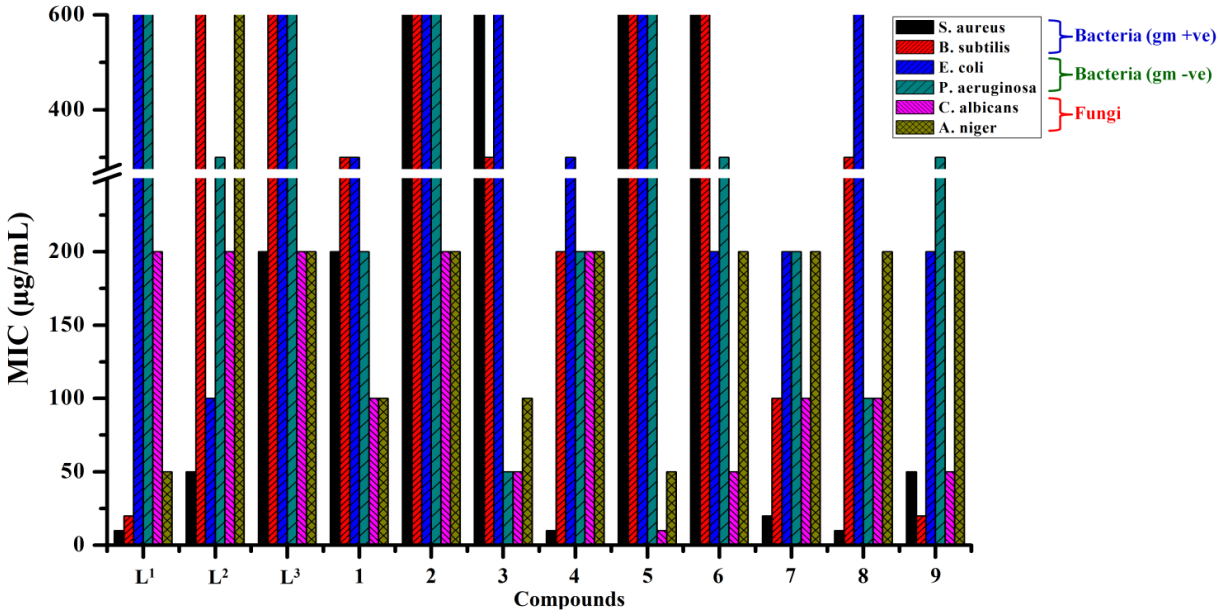

Fig. 9. Antimicrobial MIC ($\mu g ml^{-1}$) values for $\mathbf{L^1}$-$\mathbf{L^3}$ and complexes **1-9**.

All the complexes of Co(III), Ni(II) and Cu(II) derived from ligand precursors $\mathbf{L^2}$ and $\mathbf{L^3}$ are found to be less active against all the investigated bacteria, except the Cu(II)

complex **8** with MIC = 10 μgml^{-1} against S. aureus, displayed outstanding antibacterial activity. The Zn(II) complex **9** exhibited good activity against the tested bacteria. In conclusion, a number of ferrocenyl bearing compounds *viz.* **L^{1}**, **4** and **8** exhibits enhanced antibacterial activity against S. aureus (MIC = 10 μgml^{-1}) and proved to be a more potent antibacterial agent than ciprofloxacin (MIC = 15 μgml^{-1}), a well known drug.

On the other hand, the results of anti-fungal activity (Table 5) reveal that **L^{1}–L^{3}** exhibit moderate to good activity against C albicans and A. niger, except activity of **L^{1}** (very good; MIC = 50 μgml^{-1}) and **L^{2}** (poor; MIC = 600 μgml^{-1}) against against A. niger. The activity of a majority of complexes against both of the fungi is found to be very good. Remarkably, Ni(II) complex **5** appeared to exhibit excellent activity against C. albicans (MIC = 10 μgml^{-1}) and proved to be more potent antifungal agent than Flucanazole (MIC = 40 μgml^{-1}), a well known antifungal drug, as well as this complex indeed displayed enhanced antifungal activity against A niger (MIC = 50 μgml^{-1}) The mutual effect of dominant redox-active ferroceyl moieties and electron withdrawing *N*-(1-naphthylmethyl)-/ *N*-(furylmethyl)- substituents, apparently brings about superior electrochemical efficiencies in **L^{1}** and **8** and thus leading to extreme potent activity against gram positive bacteria S. aureus.

Table 5. *In vitro* antimicrobial activity of synthesized compounds **L^{1}-L^{3}** and **1-9**.

Entry	MIC (μgml^{-1})					
	(gm +ve bacteria)		(gm -ve bacteria)		(Fungi)	
	S. aureus	B. subtilis	E. coli	P. aeruginosa	C. albicans	A. niger
L^{1}	10	20	>600	>600	200	50
L^{2}	50	600	100	300	200	600
L^{3}	200	600	600	600	200	200
1	200	300	300	200	100	100
2	>600	>600	600	600	200	200
3	>600	300	>600	50	50	100
4	10	200	300	200	200	200
5	>600	600	600	600	10	50
6	>600	>600	200	300	50	200
7	20	100	200	200	100	200
8	10	300	>600	100	100	200
9	50	20	200	300	50	200
Ciprofloxacin	15	5	15	10	-	-
Flucanazole	-	-	-	-	10	40

Reports suggest that thiocarbamate derivatives disturbed the cell wall biosynthesis of the pathogen by inhibiting the ergosterol biosynthesis [41]. The activity of the metal complexes against the tested fungi may either be associated with cell wall destruction [42] DNA damage [43] protein synthesis inhibition or chelation with metal ions in fungal cells thus depriving them of the needed ions which would lead to cell mortality [44].

(a) (b) (c)

Fig. 10. Inhibition zone of $\mathbf{L^1}$ (a), **4** (b) and **8** (c) against S. Aureus in different concentration ranging from 10 µg to 600 µg/ml in DMSO solution.

2.3. Conclusion

This study allows us to conclude that a facile single pot reaction of functionalized secondary amine precursors $\mathbf{L^1}$-$\mathbf{L^3}$ with CS_2 and transition metal ion Co(III), Ni(II), Cu(II) or Zn(II) in triethylamine solvent affords access to a series of transition metal dithiocarbamate complexes **1-9**. These complexes evidently display a single quasi-reversible cyclic voltammograms due to the dominant redox-active ferrocenyl moieties in the potential range of 407 to 224 mV. The oxidation potential of the oxidizing moiety ferrocene can be modulated by changing the electronic nature of the *N*-substituents and transition metal ions. Notably, single crystal study helps to identify a new polymorphic form **8** and to realize that S/lp···π interactions playing an important role in crystal packing of **8**. Distinctly, Zn(II) complex **9** exhibits maximum fluorescence emissions at two wavelengths with concomitant Stokes shifts of 82, 200 nm, when excited at higher energy band 267 nm. Obviously, the incorporation of ferrocenyl groups potentiate the antimicrobial properties of many investigated compounds. The better potential of a number of compounds *viz.* $\mathbf{L^1}$ (against S aureus; MIC = 10 μgml^{-1}), **2** (C. albicans, MIC = 10 μgml^{-1}), **4** (against S aureus; MIC = 10 μgml^{-1}) **8** (against S aureus; MIC = 10 μgml^{-1}) than the standard reference drugs

Ciprofloxacin and Flucanazole would add merit to this work. S. aureus and P. aeruginosa are the major causes of nosocomial infections as well as community-acquired infections and C. albicans remains the predominant cause of invasive candidiasis. The outstanding antimicrobial properties of this class of compounds deserve further investigation in order to clarify the mode of action at the molecular level.

2.4. Experimental section

2.4.1. Materials and measurements

All solvents were purchased from the commercial sources and were freshly distilled prior to use. All the reagents such as metal acetates $Co(OAc)_2.4H_2O$, $Ni(OAc)_2.4H_2O$, $Cu(OAc)_2.H_2O$, $Zn(OAc)_2.2H_2O$ and CS_2 were purchased from Merck and Sigma-Aldrich Chemicals Limited, these were used without further purification. Elemental analyses (C, H, N) were carried out on a Perkin-Elmer 2400 analyzers. Thin Layer Chromatography was performed on Merck 60 F254 Aluminium coated plates. Melting points are uncorrected and were measured in open capillary tubes. FT-IR spectra were recorded in the 4000-400 cm^{-1} range using a Perkin-Elmer FT-IR spectrometer as KBr pellets. The ^{1}H and ^{13}C NMR spectra of relevant compounds were obtained on a Bruker AV-III 400 MHz spectrometer in spectrometer with $CDCl_3$ and DMSO-d_6 as solvent and TMS as internal standard. Mass spectra were recorded on Thermo-Fischer DSQ II GCMS instrument. UV-visible spectra were recorded on a Perkin Elmer Lambda 35 UV-visible spectrophotometer and the optical characterization of solid samples was performed by using the UV-visible transmittance measurements. Fluorescence was recorded on JASCO make spectrofluorometer model FP-6300. TGA/DTA plots were obtained using SII TG/DTA 6300 in flowing N_2 with a heating rate of 10 °C min^{-1}. ESI MS were obtained from AB SCIEX, 3200 Q TRAP LC/MS/MS system. Electrochemical measurements were performed on a CH Instruments 600C potentiostat, using a Pt disk as the working electrode, Ag/AgCl as the reference electrode and a Pt wire as the counter electrode. Voltammograms were recorded by using anhydrous solutions of the metal complexes in CH_2Cl_2 (1.0 mM) containing tetra-n-butylammoniumhexafluoro phosphate (0.1M) as supporting electrolyte. Magnetic Moments were done by Faraday Valance-2002 (1.0 Tesla), balance-Mettler UMx5, Temperature Controller OMEGA.

The antimicrobial activity was performed by Division of Centralnkashiba, Advanced diagnostic laboratory, Surat, India.

2.4.2. Synthesis of N-methyl-(1-naphthyl)-N-methylferrocenyl amine (L^1)

Ferrocenyl methanamine (0.864 g, 4 mmol) and 1-naphthaldehyde (0.624 g, 4 mmol) were dissolved in 40 ml toluene and the solution was refluxed for 4 h. To remove water from the reaction mixture, Dean–Stark apparatus was used; it driving the reaction to completion. Toluene was removed under vacuum and the resulting oily solid was redissolved in 50 ml ethanol and reduced with $NaBH_4$ (0.456 g, 12 mmol) by adding in 4 fractions. The reaction mixture was stirred for 8 h under nitrogen. Ethanol was removed in rotatory evaporator and the residue was dissolved in 50 ml of 50 % HCl in water and then basified the solution by saturated solution of Na_2CO_3. The product was extracted with CH_2Cl_2 (50 ml), washed with water and finally dried under vacuum to yield a light yellow oily product.

^{1}H NMR (400 MHz, DMSO-d_6): δ 2.4 (s, 1 H,–N*H*), 4.14 (s, 2 H, CH_2Fc), 4.21–4.24 (m, 7 H, Cp), 4.29-4.30 (m, 2 H, Cp), 4.51–4.53 (s, 2 H, C$H_2C_{10}H_7$), 7.57–7.63 (m, 3 H, $C_{2,3,6}H$ naphthyl), 7.67–7.69 (m, 1 H, C_7H naphthyl), 7.99–8.04 (m, 3 H, $C_{4,5,8}H$ naphthyl). ^{13}C NMR (400 MHz, DMSO-*d6*): δ 131.4, 129.1, 127.1, 126.7, 125.8, 123.9, 71.0, 69.2, 69.1, 47.3, 46.3. DEPT 135 NMR (400 MHz, DMSO-d_6): δ 130.0 (*C*H), 129.3 (*C*H), 129.1 (*C*H), 127.2 (*C*H), 126.7 (*C*H), 125.8 (*C*H), 123.9 (*C*H), 71.2 (*C*H), 69.3 (*C*H), 69.2 (*C*H), 47.2 (*C*H_2), 46.3 (*C*H_2). IR (KBr): υ = 3349 (N–H), 3093 (C–H), 1104 (C–N) cm^{-1}; (Yield 72%; Mp. 180°C)

2.4.3. Synthesis of N-methyl-(3-pyridyl)-N-methylferrocenyl amine (L^2-L^3)

Ferrocene carboxaldehyde (0.428 g, 2 mmol) and 3-picolyl amine (0.216 g, 2 mmol) or furfuryl amine (0.194 g, 2 mmol) were dissolved in 15 ml toluene and the solution was refluxed for 4 h. To remove water from the reaction mixture, Dean–Stark apparatus was used; it driving the reaction to completion. Toluene was removed under vacuum and the resulting oily solid was dissolved in 50 ml ethanol and reduced by $NaBH_4$ (0.304 g, 8 mmol) by adding in 4 fractions. The reaction mixture was stirred for 6 h under nitrogen. The ethanol was removed in rotatory evaporator and residue was redesolved in 50 ml of 50 % HCl in water and then basified by saturated solution of Na_2CO_3. Product was extracted by CH_2Cl_2 (50 ml), washed with water and then solvent was removed under vacuum to yield the oily orange product.

L^{2}*:* ^{1}H NMR (400 MHz, DMSO-d_6): δ 3.25 (s, 1 H,–N*H*), 3.73 (s, 2 H, CH_2Fc), 4.05 (s, 2 H, C$H_2C_5H_4N$), 4.08–4.20 (m, 9 H, Cp), 7.33–7.36 (dd, 1 H, C_5H pyridine), 7.74–7.76 (d, 1 H, C_4H pyridine), 8.44–8.45 (d, 1 H, C_6H pyridine), 8.53 (s, 1 H, C_2H pyridine). ^{13}C NMR (400 MHz, DMSO-d_6): δ 149.8, 148.4, 136.3, 136.1, 123.8, 86.9, 68.7, 68.7, 67.7, 50.0, 47.8. DEPT 135 NMR (400 MHz, DMSO-d_6): δ 149.8 (*C*H), 148.4(*C*H), 136.1(*C*H), 123.8 (*C*H), 68.7 (*C*H), 68.7 (*C*H), 67.7 (*C*H), 50.0 (CH_2), 47.8 (CH_2). IR (KBr): υ = 3282 (N–H), 3080 (C–H), 1084 (C–N) cm^{-1}; (Yield 75%; Mp. 50°C)

L^{3}*:* ^{1}H NMR (400 MHz, DMSO-d_6): δ 2.24 (s, 1 H,–N*H*), 3.67 (s, 2 H, CH_2Fc), 4.06 (s, 2 H, C$H_2C_4H_3O$), 4.09–4.19 (m, 9 H, Cp), 6.25 (d, 1 H, C_3H furan), 6.38–6.40 (dd, 1 H, C_4H furan), 7.57–7.58 (dd, 1 H, C_5H furan). ^{13}C NMR (400 MHz, DMSO-d_6): δ 154.7, 142.2, 110.7, 107.1, 87.2, 68.6, 68.5, 67.6, 47.6, 45.3. DEPT 135 NMR (400 MHz, DMSO-d_6): δ 142.2 (*C*H), 110.7 (*C*H), 107.1 (*C*H), 68.6 (*C*H), 68.5 (*C*H), 67.6 (*C*H), 47.6 (CH_2), 45.3 (CH_2). IR (KBr): υ = 3323(N–H), 3093 (C–H), 1147 (C–N) cm^{-1}; (Yield 74%; Mp. 45°C)

2.4.4. Synthesis of [M{κ^2S,S-$S_2CN(CH_2R)CH_2Fc$}$_n$] {R = 1-naphthyl, 3-pyridyl or 2-furyl (n = 2 or 3} (1-9)

The ligand precursors, *N*-methyl-(1-naphthyl)-*N*-methylferrocenyl amine (**L^1**) (0.355 g, 1.0 mmol), *N*-methyl-(3-pyridyl)-*N*-methylferrocenyl amine (**L^2**) (0.306 g, 1.0 mmol) or *N*-furfuryl-*N*-methylferrocenyl amine (**L^3**) (0.295 g, 1.0 mmol), was dissolved in 20 ml of triethyl amine and then after 30 minutes CS_2 (0.228 g, 3.0 mmol) were added. The mixture was stirred for 1hr and then $Co(OAc)_2.4H_2O$ (0.084 g, 0.33 mmol), $Ni(OAc)_2.4H_2O$ (0.124 g, 0.5 mmol), $Cu(OAc)_2.H_2O$ (0.101 g, 0.5 mmol) or $Zn(OAc)_2.2H_2O$ (0.110 g, 0.5 mmol) was added. The mixture was stirred 6-7 hrs then concentration the reaction mixtures then precipitate comes. Filter it and washed the residue with petroleum ether and distilled water three to four times. Collect the residue and after drying in high vacuum store the solid powder in 10-20 ºC under nitrogen atmosphere. Compound **1** Green solid (0.348 g, 0.257 mmol, 78% yield); Mp. 295−302 °C (decomposes). MS (LC): *m/z* 1351.1 $[M+H]^+$. IR (KBr): υ = 3080 (C–H), 1460 (C=N), 1147 (C–N), 991 (C–S) cm^{-1}; elemental Anal. Calcd (%) for $C_{69}H_{60}Fe_3N_3S_6Co$ (M.W. 1350.6): C 61.38, H 4.48, N 3.11, S 14.25; Found: C 61.41, H 4.45, N 3.09, S 14.13.

Compound **2** Green solid (0.338 g, 0.281 mmol, 85% yield); Mp: 241−245°C (decomposes); ^{1}H NMR (400 MHz, DMSO-d_6): δ 4.10-4.19 (m, 18 H, Cp), 4.22-4.24 (m, 9 H, Cp), 4.65 (s, 6 H, CH_2Fc), 4.88 (s, 6 H, CH_2C$_5$H$_4$N), 7.48 (s, 3 H, C$_5$*H* pyridine), 7.64 (s, 3 H, C$_4$*H* pyridine), 8.67 (d, 6 H, C$_{2,6}$*H* pyridine). MS (ESI): *m/z* 1202.65 $[M]^+$. IR (KBr): υ = 3028 (C–H), 1480 (C=N), 1104 (C–N), 1026 (C–S) cm^{-1}; elemental Anal. Calcd (%) for $C_{54}H_{51}Fe_3N_6S_6Co$ (M.W. 1202.4): C 53.92, H 4.27, N 6.99, S 15.99; Found: C 53.87, H 4.24, N 6.95, S 15.94.

Compound **3** Green solid (0.325 g, 0.277 mmol, 84% yield); Mp. 235−241 °C (decomposes); ^{1}H NMR (400 MHz, DMSO-d_6): δ 4.20-4.21 (s, 18 H, Cp), 4.37-4.41 (s, 9 H, Cp), 4.58 (s, 6 H, CH_2Fc), 4.78 (s, 4 H, CH_2C$_4$H$_3$O), 6.49 (s, 6 H, C$_{3,4}$*H* furan), 7.68 (d, 3 H, C$_5$*H* furan). MS (LC): *m/z* 1169.1 $[M]^+$. IR (KBr): υ = 3088 (C–H), 1478 (C=N), 1146 (C–N), 1013 (C–S) cm^{-1}; elemental Anal. Calcd (%) for $C_{51}H_{48}Fe_3N_3O_3S_6Co$ (M.W. 1169.8): C 52.36, H 4.14, N 3.57, S 16.41; Found: C 52.36, H 4.14, N 3.59, S 16.45.

Compound **4** Green solid (0.368 g, 0.400 mmol, 80% yield); Mp. 229−234 °C (decomposes); ^{1}H NMR (400 MHz, DMSO-d_6): δ 4.12–4.26 (m, 18 H, Cp), 4.55 (s, 4 H, CH_2Fc), 5.20 (s, 4 H, CH_2C$_{10}$H$_7$), 7.20 (s, 2 H, C$_2$H naphthyl), 7.58 (s, 6 H, C$_{3,6,7}$*H* naphthyl), 7.81–7.98 (m, 2 H, C$_{4,5,8}$*H* naphthyl). DEPT 135 NMR (400 MHz, DMSO-d_6): δ 129.2 (*C*H), 128.8 (*C*H), 127.1 (*C*H), 126.6 (*C*H), 125.9 (*C*H), 125.1 (*C*H), 123.3 (*C*H), 70.2 (*C*H), 69.0 (*C*H), 68.8 (*C*H), 50.0 (*C*H$_2$), 49.0 (*C*H$_2$). MS (LC): *m/z* 918.1 $[M]^+$. IR (KBr): υ = 3086 (C–H), 1494 (C=N), 1141 (C–N), 999 (C–S) cm^{-1}; elemental Anal. Calcd (%) for $C_{46}H_{40}Fe_2N_2S_4Ni$ (M.W. 919.4): C 60.09, H 4.38, N 3.05, S 13.95; Found: C 60.13, H 4.39, N 3.07, S 13.92.

Compound **5** Green solid (0.361 g, 0.439 mmol, 88% yield); Mp: 235−240 °C (decomposes); ^{1}H NMR (400 MHz, DMSO-d_6): δ 4.184 (m, 14 H, Cp), 4.35 (m, 4 H, Cp), 4.55 (s, 4 H, CH_2Fc), 4.77 (s, 4 H, CH_2C$_5$H$_4$N), 7.40 (m, 2 H, C$_5$*H* pyridine), 7.60 (m, 2 H, C$_4$*H* pyridine), 8.45-8.52 (d, 4 H, C$_{2,6}$*H* pyridine). MS (ESI): *m/z* 820.94 $[M+H]^+$. IR (KBr): υ = 3088 (C–H), 1492 (C=N), 1105 (C–N), 1027 (C–S) cm^{-1}; elemental Anal. Calcd (%) for $C_{36}H_{34}Fe_2N_4S_4Ni$ (M.W. 820.3): C 52.64, H 4.17, N 6.82, S 15.62; Found: C 52.65, H 4.16, N 6.80, S 15.60.

Compound **6** Green solid (0.356 g, 0.445 mmol, 89% yield); Mp. 198−205 °C; ^{1}H NMR (400 MHz, DMSO-d_6): δ 4.19 (s, 14 H, Cp), 4.34 (s, 4 H, Cp), 4.48 (s, 4 H, CH_2Fc), 4.69 (s, 4 H, CH_2C$_4$H$_3$O), 6.49 (s, 4 H, C$_{3,4}$*H* furan), 7.70 (2 d, H, C$_5$*H* furan). MS (LC): *m/z* 799.7 $[M+H]^+$. IR (KBr): υ = 3090 (C–H), 1488 (C=N), 1148

(C–N), 1012 (C–S) cm^{-1}; elemental Anal. Calcd (%) for $C_{34}H_{32}Fe_2N_2O_2S_4Ni$ (M.W. 799.2): C 51.09, H 4.04, N 3.50, S 16.05; Found: C 51.07, H 4.02, N 3.49, S 16.02.

Compound **7** Brown solid (0.374 g, 0.404 mmol, 81% yield); Mp. 287−292 °C (decomposes). MS (LC): *m/z* 923.1 $[M]^+$ IR (KBr): υ = 3046 (C–H), 1476 (C=N), 1197 (C–N), 1000 (C–S) cm^{-1}; elemental Anal. Calcd (%) for $C_{46}H_{40}Fe_2N_2S_4Cu$ (M.W. 923.3): C 59.77, H 4.36, N 3.03, S 13.88; Found: C 59.80, H 4.39, N 3.01, S 13.90.

Compound **8** Brown solid (0.342 g, 0.423 mmol, 85% yield); Mp. 205−208 °C. MS (LC): *m/z* 804.7 $[M+H]^+$. IR (KBr): υ = 3088 (C–H), 1144 (C–N), 1488 (C=N), 1016 (C–S) cm^{-1}; elemental Anal. Calcd (%) for $C_{34}H_{32}Fe_2N_2O_2S_4Cu$ (M.W. 804.1): C 50.78, H 4.01, N 3.48, S 15.95; Found: C 50.75, H 4.02, N 3.47, S 15.96.

Compound **9** Light Yellow solid (0.403 g, 0.435 mmol, 87% yield); Mp. 105−109 °C (decomposes); ^{1}H NMR (400 MHz, DMSO-d_6): δ 4.06 (m, 14 H, Cp), 4.37-4.38 (m, 4 H, Cp), 5.06 (s, 4 H, CH_2Fc), 5.80 (s, 4 H, C$H_2C_{10}H_7$), 7.20 (m, 2 H, C_2H naphthyl), 7.46-7.53 (m, 6 H, $C_{3,6,7}H$ naphthyl), 7.81 (m, 2 H, C_4H naphthyl), 7.7.94 (m, 2 H, C_5H naphthyl), 8.12 (m, 2 H, C_8H naphthyl). ^{13}C NMR (400 MHz, DMSO-d_6): δ 207.0 (CS_2), 134.2, 133.8, 131.6, 128.9, 127.2, 126.4, 126.0, 125.9, 124.8, 124.0, 85.1, 70.2, 68.6, 67.6, 52.3, 49.6, 46.1.; DEPT 135 NMR (400 MHz, DMSO-d_6): δ 133.6 (CH), 131.1 (CH), 130.8 (CH), 130.6 (CH), 129.5 (CH), 128.7 (CH), 74.9 (CH), 73.6 (CH), 73.4 (CH), 72.3 (CH), 50.8 (CH_2). MS (LC): *m/z* 924.0 $[M]^+$ IR (KBr): υ = 3090 (C–H), 1463 (C=N), 1144 (C–N), 1019 (C–S) cm^{-1}; elemental Anal. Calcd (%) for $C_{46}H_{40}Fe_2N_2S_4Zn$ (M.W. 925.1): C 59.65, H 4.35, N 3.02, S 13.85; Found: C 59.45, H 4.32, N 3.05, S 13.90.

2.5. References

1. Kealy, T. J.; Pauson, P. L. *Nature* **1951**, *168*, 1039.
2. (a) Wong, W. W. H.; Curiel, D.; Lai, S.-W.; Drew, M. G. B.; Beer, P.D. *Dalton Trans*. **2005**, 774; (b) Lai, S.-W.; Drew, M. G. B.; Beer, P. D. *J. Organomet. Chem*. **2001**, *637*, 89.
3. (a) Kumar, A.; Chauhan, R.; Molloy, K. C.; Kociok-Kçhn, G.; Bahadur, L.; Singh, N. *Chem. Eur. J.* **2010**, *16*, 4307; (b) Singh, V.; Chauhan, R.; Gupta, A. N.; Kumar, V.; Drew, M. G .B.; Bahadur, L.; Singh, N. *Dalton Trans*. **2014**, *43*, 4752.

4. (a) van Stavern, D. R.; Metzler-Nolte, N. *Chem. Rev.* **2004**, *104*, 5931; (b) Gasser, G.; Ott, I.; Metzler-Nolte, N. *J. Med. Chem.* **2011**, *54*,3; (c) Patra, M.; Gasser, G.; Metzler-Nolte, N. *Dalton Trans*. **2012**, *41*, 6350; (d) Ornelas, C. *New J. Chem.* **2011**, *35*, 1973; (e) Patra, M.; Gasser, G.; *ChemBioChem*. **2012**, *13*, 1232; (f) Biot, C.; François, N.; Maciejewski, L.; Brocard, J.; Poulain, D. *Bioorg. Med. Chem. Lett*. **2000**, *10*, 839; (g) Chantson, J. T.; Verga, F. M. V.; Crovella, S.; Metzler-Nolte, N. *ChemMedChem*, **2006**, *1*, 1268. (h) Tirkey, V.; Mishra, S.; Dash, H. R.; Das, S.; Nayak, B. P.; Mobin, S. M.; Chatterjee, S. *J. Organomet. Chem*. **2013**, *732*, 122.

5. (a) Hillard, E. A.; Vessières, A.; Thouin, L.; Jaouen, G.; Amatore, C. *Angew. Chem. Int. Ed.* **2006**, *45*, 285; (b) Hamels, D.; Dansette, P.; Hillard, E .A.; Top, S.; Pigeon, P.; Jaouen, G.; Mansuy, D. *Angew. Chem. Int. Ed.* **2009**, *48*, 9124.

6. (a) Biot, C.; Daher, W.; Chavain, N.; Fandeur, T.; Khalife, J.; Dive, D.; Clerq, E .D. *J. Med. Chem.* **2006**, *49*, 2845; (b) Delhaes, L.; Biot, C.; Berry, L.; Delcourt, P.; Maciejewski, L.; Camus, D.; Brocard, J. S.; Dive, D. *ChemBioChem*, **2002**, *3*, 418.

7. (a) Edwards, E. I.; Epton, R.; Marr, G. *J. Organomet. Chem*. **1975**, *85*, C23; (b) Edwards, E. I.; Epton, R.; Marr, G. *J. Organomet. Chem*. **1976**, *122*, C49; (c) Edwards, E. I.; Epton, R.; Marr, G. *J. Organomet. Chem*. **1979**, *168*, 259.

8. (a) Bousseau, M.; Valade, L.; Legros, J. P.; Cassoux, P.; Garbaukas, M.; Interrante, L. V. *J. Am. Chem. Soc*. **1986**, *108*, 1908; (b) Coomber, A. T.; Beljonne, D.; Friend, R. H.; Bredas, J. L.; Charlton, A.; Robertson, N.; Underhill, A. E.; Kurmoo, M.; Day, P. *Nature*, **1996**, *380*, 144; (c) Singh, N.; Singh, V. K. *Trans. Met. Chem*. **2001**, *26*, 435; (d) Wilton-Ely, J. D. E. T.; Solanki, D.; Knight, E .R.; Holt, K. B.; Thompson, A. L.; Hogarth, G. *Inorg. Chem*. **2008** , *47*, 9642; (e) Wilton-Ely, J. D. E. T.; Solanki, D.; Hogarth, G.; *Eur. J. Inorg. Chem.* **2005**, 4027.

9. (a) Banerjee, S.; Kumar, G .R.; Mathur, P.; Sekar, P. *Chem. Commun*. **1997**, 299; (b) Mathur, P.; Rai, D.K.; Shyam Ji, R.; Pathak, B.; Boodida, S.; Mobin, S. M. *RSC Adv*. **2013**, *3*, 26025; (c) Mathur, P.; Mukhopadhyay, S.; Ahmed, M. O.; Lahiri, G. K.; Chakraborty, S.; Walawalkar, M. G.; *Organometallics*, **2000**, *19*, 5787; (d) Gupta, R. Pandey, R. K.; Singh, R.; Srivastava, N.; Maiti, B.; Saha, S.; Li, P.; Xu, Q.; Pandey, D.S. *Inorg. Chem*. **2012**, *51*, 8916.

10. Tisdale, W. H.; Williams, I. *Disinfectant, US*, **1972**, *96*, 1934.

11. (a) Kumar, L.; Sarswat, A.; Lal, N.; Sharma, V. L.; Jain, A.; Kumar, R.; Verma, V.; Maikhuri, J. P.; Kumar, A.; Shukla, P. K.; Gupta, G. *Eur. J. Med*. Chem. **2010** , *45*, 817; (b) Jangir, S.; Bala, V.; Lal, N.; Kumar, L.; Sarswat, A.; Kumar, L.; Kushwaha, B.; Singh, P.; Shukla, P. K.; Maikhuri, J. P.; Gupta, G.; Sharma, V. L. *Org. Biomol. Chem*. **2014**, *12*, 3090.
12. Wood, T. F.; Gardner, J. H. *J. Am. Chem. Soc*. **1941 ,** *63*, 2741.
13. Spallarossa, A.; Cesarini, S.; Ranise, A.; Bruno, O.; Schenone, S.; La Colla, P.; Collu, G.; Sanna, G.; Secci, B.; Loddo, R. *Eur. J. Med. Chem.* **2009** , *44*, 2190.
14. Kapa, N. C.; Muccioli, G. G.; Labar, G.; Poupaert, J. H.; Lambert, D. M. *J. Med. Chem*. **2009** , *52*,7310.
15. Huang, W.; Ding, Y.; Miao, Y.; Liu, M.-Z.; Li, Y.; Yang, G.-F. *Eur. J. Med. Chem*. **2009**, *44*, 3687.
16. Westrop, G. D.; Georg, I.; Coombs, G. H. *J. Biol. Chem*. **2009** , *284*, 33485.
17. Spellberg, B.; Powers, J. H.; Brass, E. P.; Miller, L. G.; Edwards, Jr. J. E. *Clin Infect Dis*. **2004** , *38*, 1279.
18. Huang, C. M.; Chen, C. H.; Pornpattananangkul, D.; Zhang, L.; Chan, M.; Hsieh, M. F.; Zhang, L. *Biomaterials*, **2011**, *32*,214.
19. Monk, B. C.; Goffeau, A. *Science*, **2008**, *321*, 367.
20. (a) Menezes, D. C.; Vieira, F. T.; de Lima, G. M.; Porto, A. O.; Cortés, M. E.; Ardisson, J. D.; Albrecht-Schmitt, T. E. *Eur. J. Med. Chem*. **2005**, *40*, 1277; (b) Arora, A.; Sud, D.; Sharma, J. R. *Chem. Asian. J*. **2003**, *15*, 715–719; (c) Mambaa, S. M.; Mishraa, A. K.; Mamba, B. B.; Njobeh, P. B.; Dutton, M. F. Fosso-Kankeu, E.; *Spectrochimica Acta Part A*, **2010**, *77*, 579.
21. (a) Singh, V. K.; Kadu, R.; Roy, H. *Eur. J. Med. Chem*. **2014**, *74*, 552; (b) Kadu, R.; Singh, V. K.; Verma, S. K.; Raghavaiah, P.; Shaikh, M. M. *J. Mol. Struct*. **2013**, *1033*, 298.
22. (a) Mamba, S. M.; Mishra, A. K.; Mamba, B. B.; Njobeh, P. B.; Dutton, M. F.; Kankeu, E. F. *Spectrochimica Acta Part A*, **2010**, *77*, 579; (b) Verma, S. K.; Singh, V. K. *Polyhedron*, **2014**, *76*, 1.
23. Valarmathi, P.; Thirumaran, S.; Ragi, P.; Ciattini, S. *J. Coord. Chem*. **2011**, *64*, 4157.
24. Abu-Eitta, R. H.; Bahgat, A. H.; El-Tawil, C. *Can. J. Chem*. **1985**, *63*, 1173.
25. (a) Wong, W. W. H.; Phipps, D. E.; Beer, P. D. *Polyhedron*, **2004** , *23*, 2821; (b) Gölcü, A.; Yavuz, P.; Russ. *J. Coord. Chem*. **2008**, *34*, 106.

26. Sohn, Y. S.; Hendrickson, D. N.; Gray, H. B. *J. Am. Chem. Soc*. **1971**, 93, 3603.
27. (a) Wilton-Ely, J. D. E. T.; Solanki, D.; Knight, E. R.; Holt, K. B.; Thompson, A. L.; Hogarth, G. *Inorg. Chem*. **2008**, *47*, 9642; (b) A. B. P. Lever in Inorganic Electronic Spectroscopy, Elsevier, Amsterdam (1984) pp. 479.
28. (a) Verma, S. K.; Kadu, R.; Singh, V. K. *Synth. React. Inorg. Met.-Org. Nano-Met. Chem*. **2014**, *44*, 441; (b) Chai, L.-Q.; Wang, G.; Sun, Y.-X.; Dong, W.-K.; Zhao, L.; Gao, X.-H. *J. Coord. Chem*. **2012** , *65*, 1621; (c) Pandey, R.; Kumar, P.; Singh, A. K.; Shahid, M.; Li, P. Z.; Singh, S. K.; Xu, Q.; Misra, A.; Pandey, D. S. *Inorg. Chem*. **2011**, *50*, 3189; (d) Kumar, V.; Singh, V.; Gupta, A. N.; Singh, S. K.; Drew, M. G. B.; Singh, N. *Polyhedron*, **2015**, *89*, 304.
29. Sreedaran, S.; Bharathi, K. S.; Rahiman, A. K.; Jagadish, L.; Kaviyarasan, V.; Narayanan, V. *Polyhedron* **2008**, *27*, 2931.
30. (a) Mizobe, Y.; Hinoue, T.; Yamamoto, A.; Hisaki, I.; Miyata, M.; Hasegawa, Y.; Tohnai, N. *Chem. Eur. J*. **2009**, *15*, 8175; (b) Lee, K.-H.; Choi, C.-S.; Jeon, K.-S.; *Photosci. J*. **2002**, *9*, 71; (c) Martens, S. C.; Zschieschang, U.; Wadepohl, H.; Klauk, H.; Gade, L. H. *Chem. Eur. J*. **2012**, *18*, 3498; (d) Valdés, A. C.; Luis, G. P.; Rivero, I. A.; *J. Mex. Chem. Soc*. **2007**, *51*, 87; (e) Madrigal, D.; Luis, G. P.; Rivero, I. A.; *J. Mex. Chem. Soc*. **2006** , *50*, 175.
31. (a) Jetti, D. R. K. R.; Boese, P. D. R.; Thallapally, D. P. K.; Desiraju, P. G. R.; Katz, A. K.; Carrell, Dr. H. L. *Angew. Chem. Int. Ed*. **2004**, *43*, 1149; (b) Bond, A. D.; Boese, R.; Desiraju, G. R. *Angew. Chem. Int. Ed*. **2007**, *46*, 618.
32. Borka, L.; Haleblian, J. K. *Acta Pharm. Jugosl*. **1990**, *40*, 71.
33. (a) Shukla, R.; Mohan, T. P.; Vishalakshic, B.; Chopra, D. *CrystEngComm*, **2014**, *16*, 1702; (b) Robertazzi, A.; Krull, F.; Knapp, E. W.; Gamez, P. *CrystEngComm*, **2011**, *13*, 3293.
34. (a) Egli, M.; Sarkhel, R. *Acc. Chem. Res*. **2007**, *40*, 197; (b) Jain, A.; Ramanathan, V.; Sankararamakrishnan, R. *Protein Sci*. **2009**, *18*, 595.
35. Yang, H.; Chen, X.; Jiang, W.; Lu, Y. *Inorg. Chem. Commun*. **2005**, 8, 853.
36. Keller, T. M.; Qadri, S. B.; *Chem. Mater*. **2004**, *16*, 1091.
37. Leonhardt, A.; Hampel, S.; Müller, C.; Mönch, I.; Koseva, R.; Ritschel, M.; Elefant, D.; Biedermann, K.; Büchner, B. *Chem. Vap. Deposition* **2006**, *12*, 380.
38. Verma, S. K.; Singh, V. K. *J. Coord. Chem*. **2015**, 1. DOI: 10.1080/00958972.2014.1003550.

39. (a) Top, S.; Tang, J.; Vessikres, A.; Carrez, D.; Provot, C.; Jaouen, G. *Chem. Commun*. **1996**, 955–956; (b) Jaouen, G.; Top, S.; Vessieres, A.; Leclercq, G.; McGlinchey, J. M. *Curr. Med.Chem*. **2004**, *11*, 2505.
40. National Committee for Clinical Laboratory Standards, Performance Standards for Antimicrobial Susceptibility Testing, 8th Informational Supplement. M100 S12, National Committee for Clinical Laboratory Standards, Villanova, Pa, 2002.
41. Ryder, N. S.; Frank, I.; Dupon, M. C. *Antimicrob. Agents Chemother*. **1986**, *29*, 858.
42. Mishra, A. K.;. Kaushik, N. K. *Spectrochimica Acta Part A* **2008**, *69*, 842.
43. Pellerito, C.; Nagy, L.; Pellerito, L.; Szorcsik, A. *J. Organomet. Chem*. **2006**, *691*, 1733.
44. (a) van den Bossche, H.; Dromer, F.; Improvissi, L.; Lozane-Chiu, M.; Hex, J. H.; Sanglard, D. *Medical Mycology*, **1998**, *36*, 119; (b) Mohammad, A.; Varshney, C.; Nami, S. A. A. *Spectrochimica Acta Part A*, **2009** , *73*, 20.

2.6. Spectra and plots

2.6.1. IR spectra

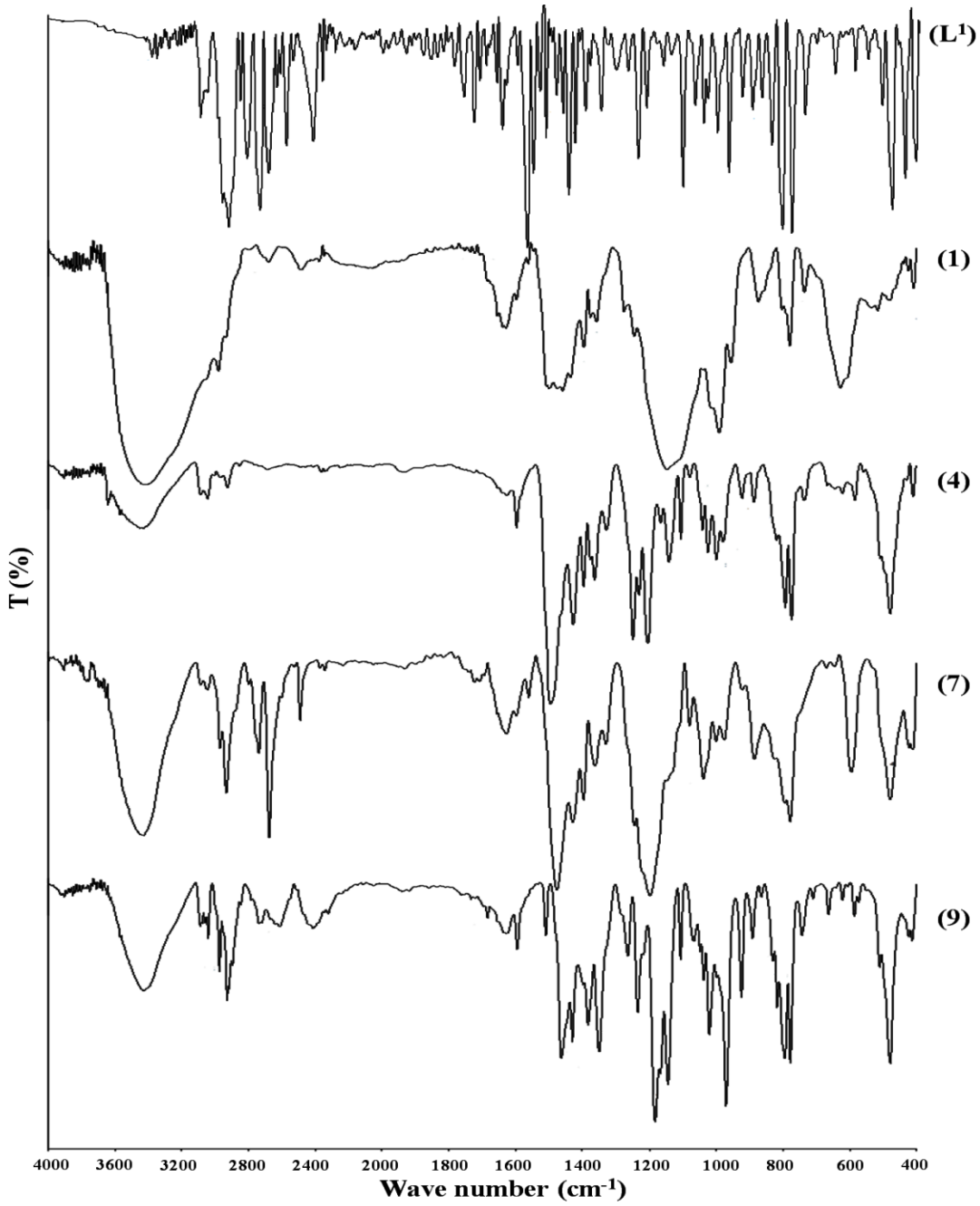

Figure S1. IR Spectrum of *N*-methyl-(1-naphthyl)-*N*-methyl ferrocenyl amine (L^1) and its complexes 1,4,7 and 9.

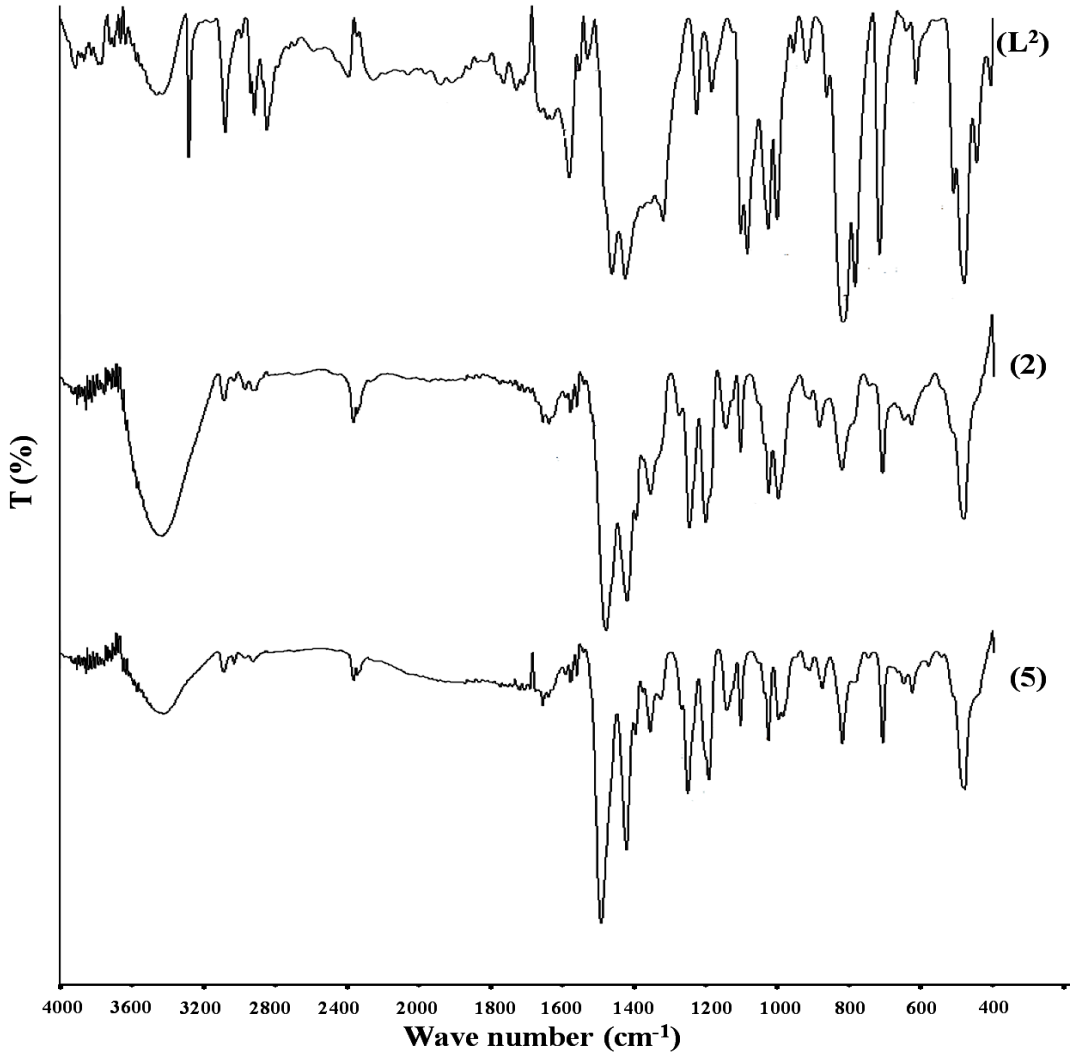

Figure S2. IR Spectrum of *N*-methyl-(3-pyridyl)-*N*-methylferrocenyl amine (L^2) and its complexes 2 and 5.

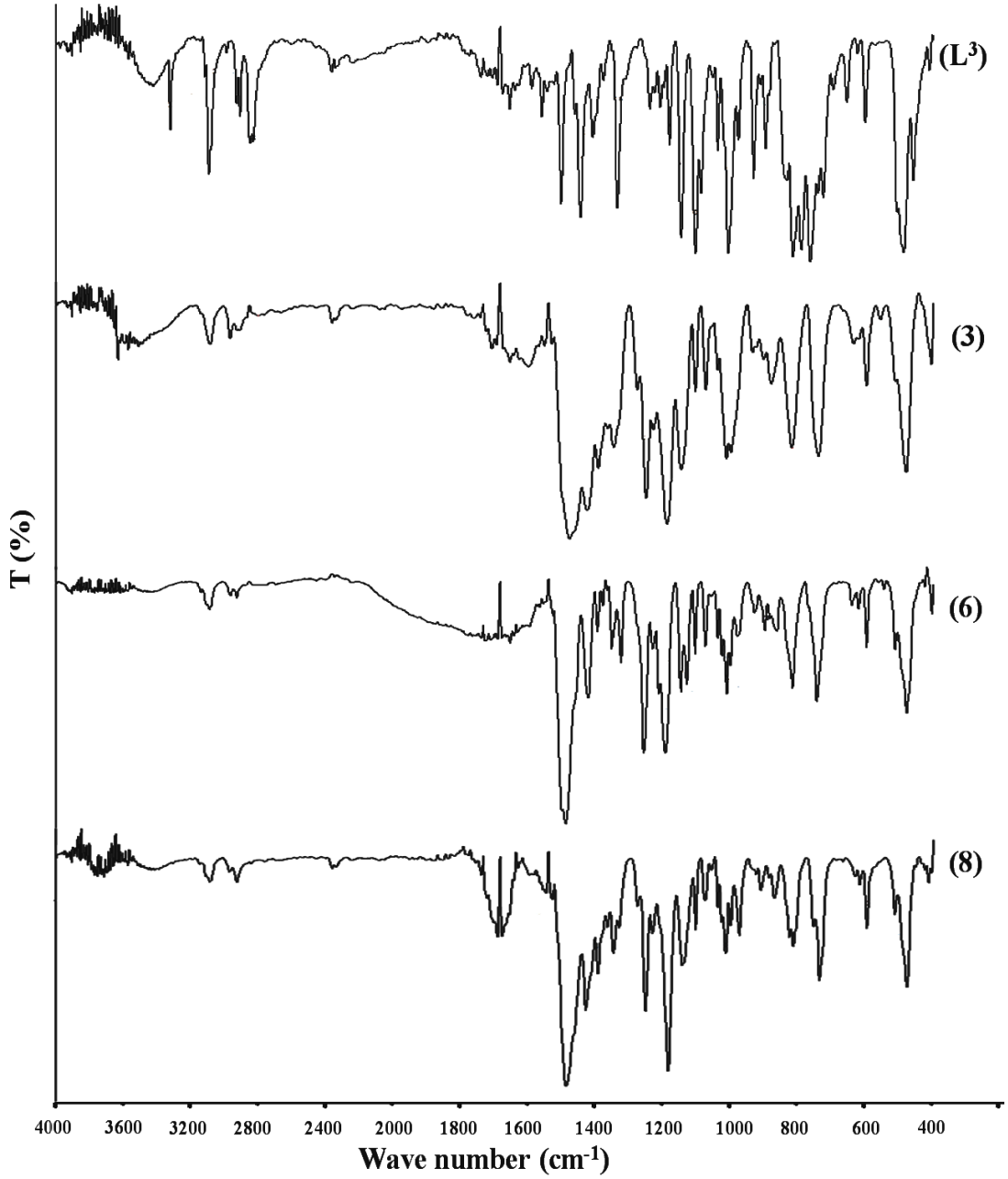

Figure S3. IR Spectrum of *N*-furfuryl-*N*-methylferrocenyl amine (L^3) and its complexes 3, 6 and 8.

2.6.2. ESI MS spectra

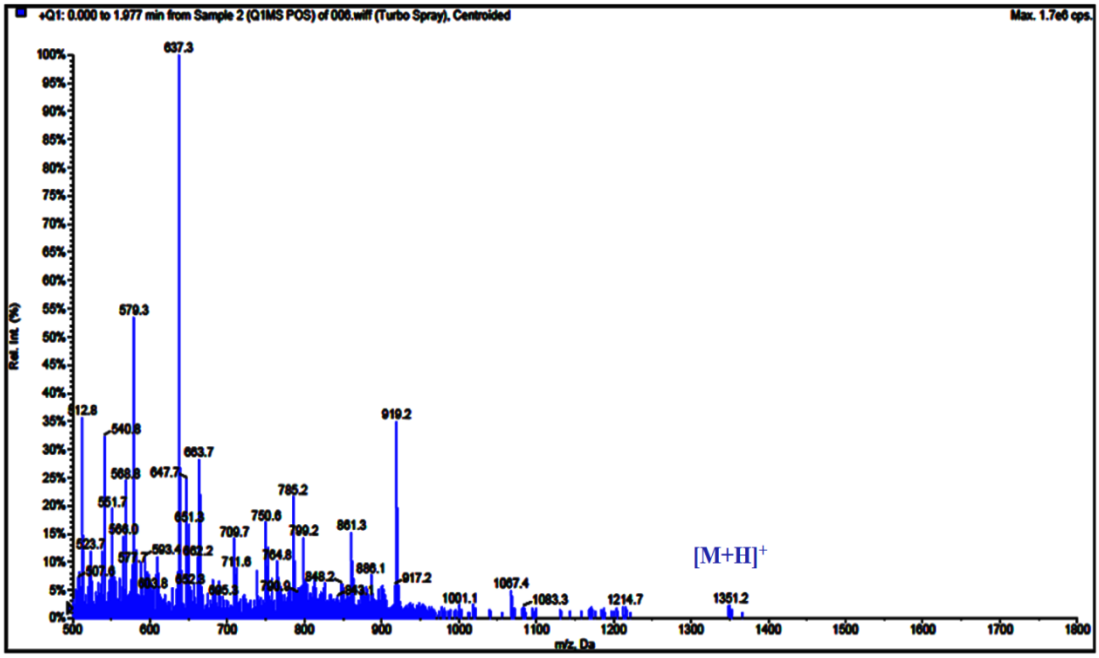

Figure S4. LC MS spectra of complex 1

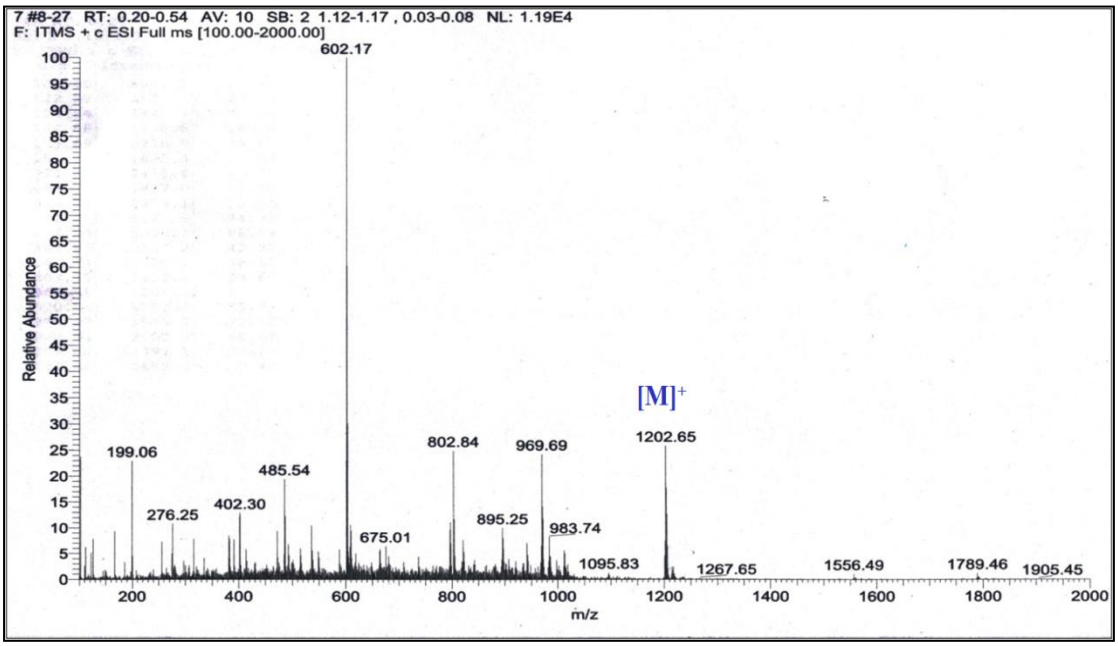

Figure S5. ESI MS spectra of complex 2

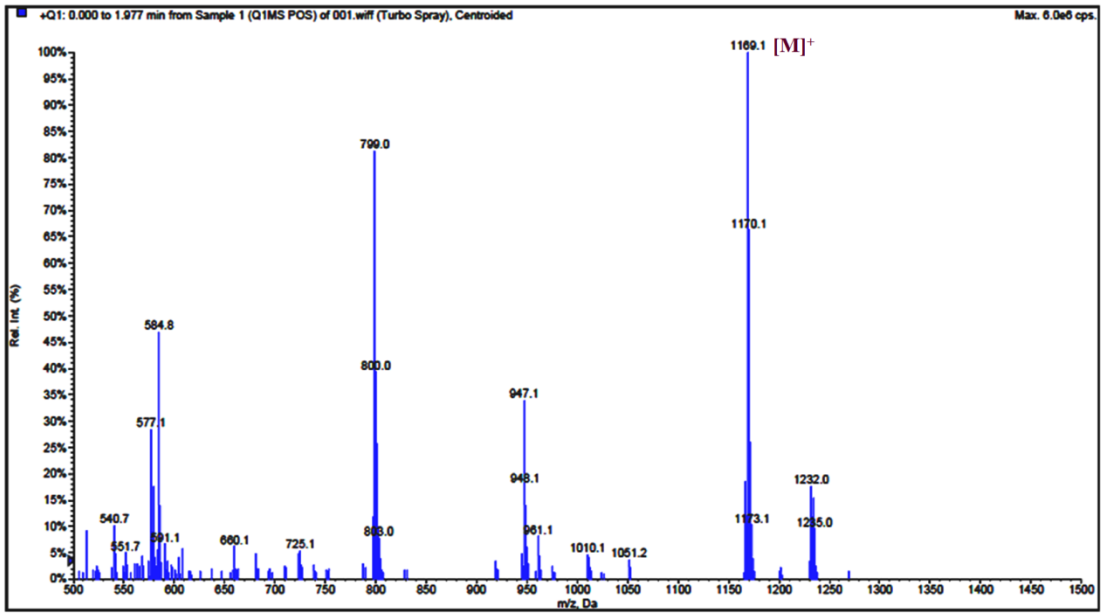

Figure S6. LC MS spectra of complex 3

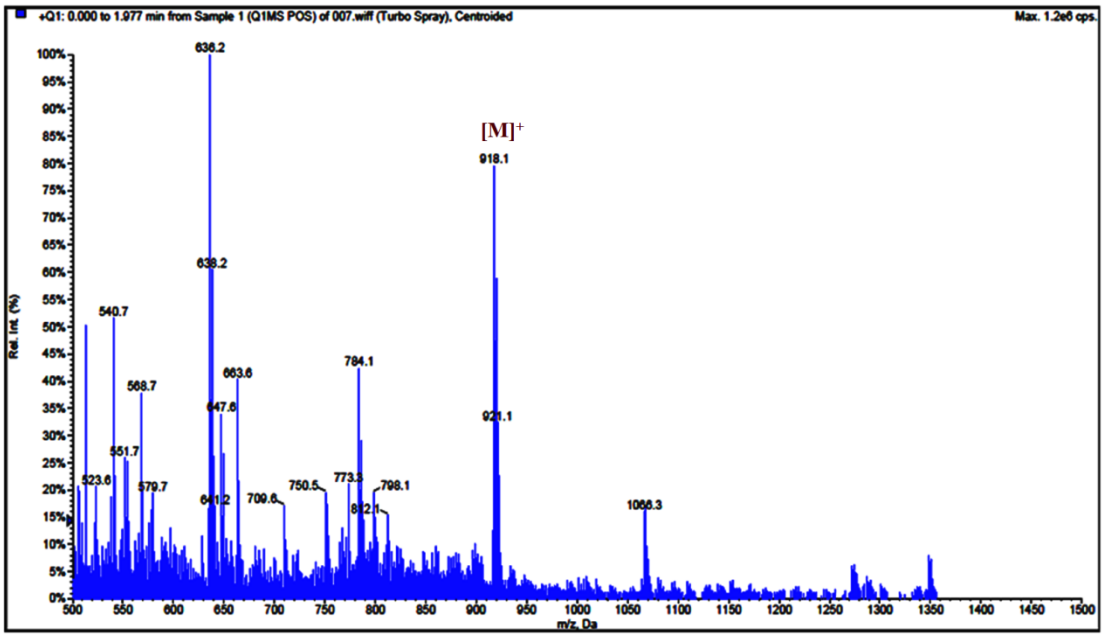

Figure S7. LC MS spectra of complex 4

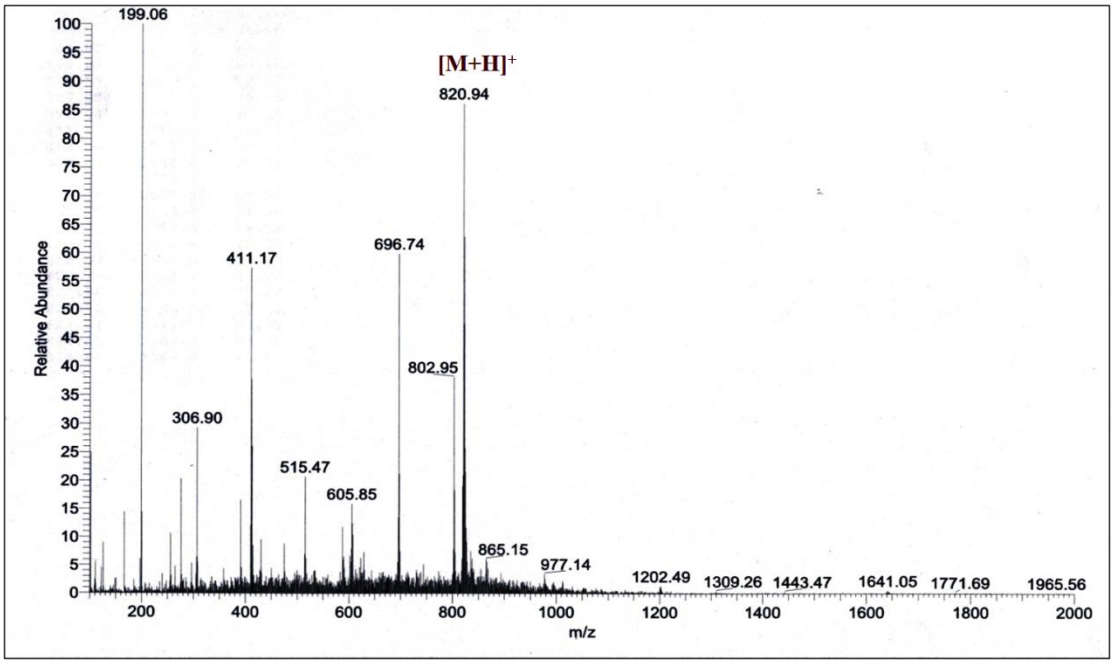

Figure S8. ESI MS spectra of complex 5

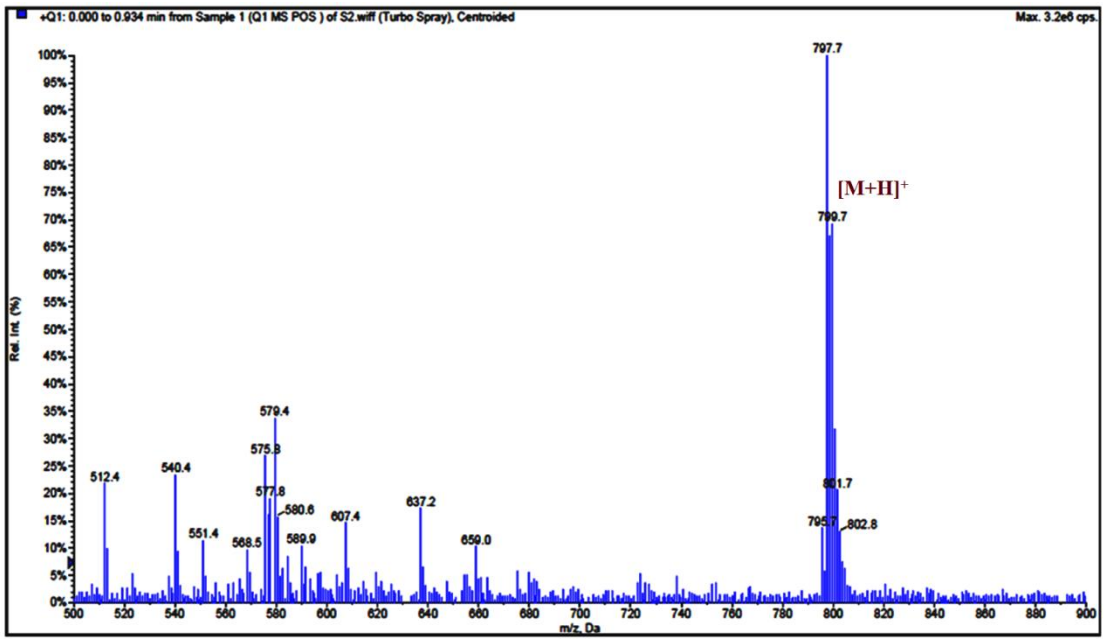

Figure S9. LC MS spectra of complex 6

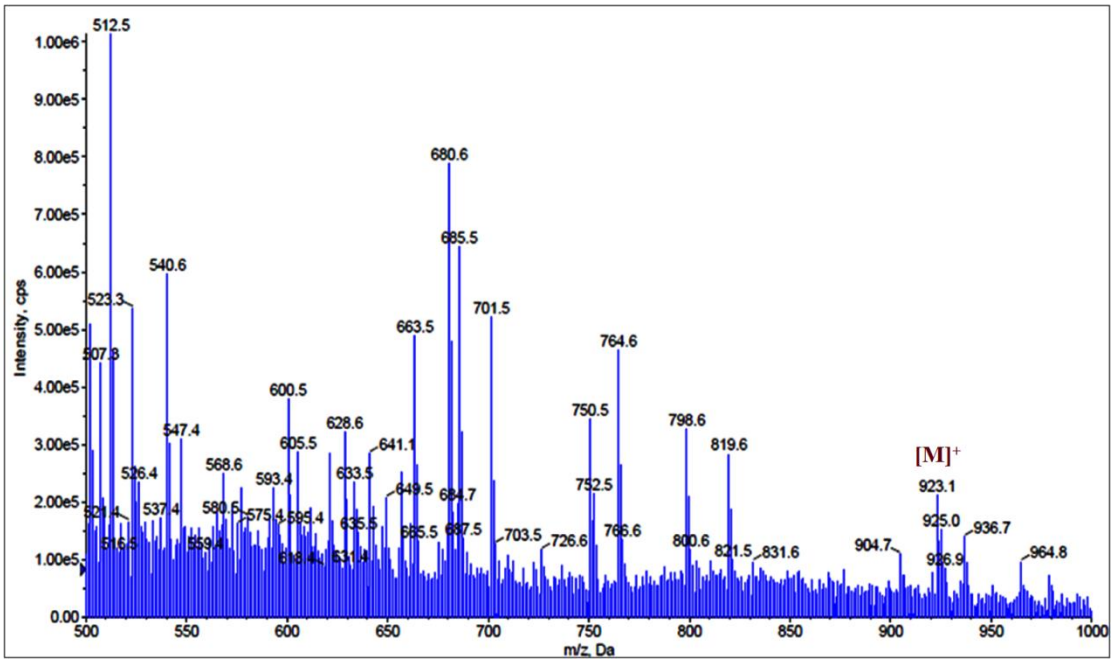

Figure S10. LC MS spectra of complex 7

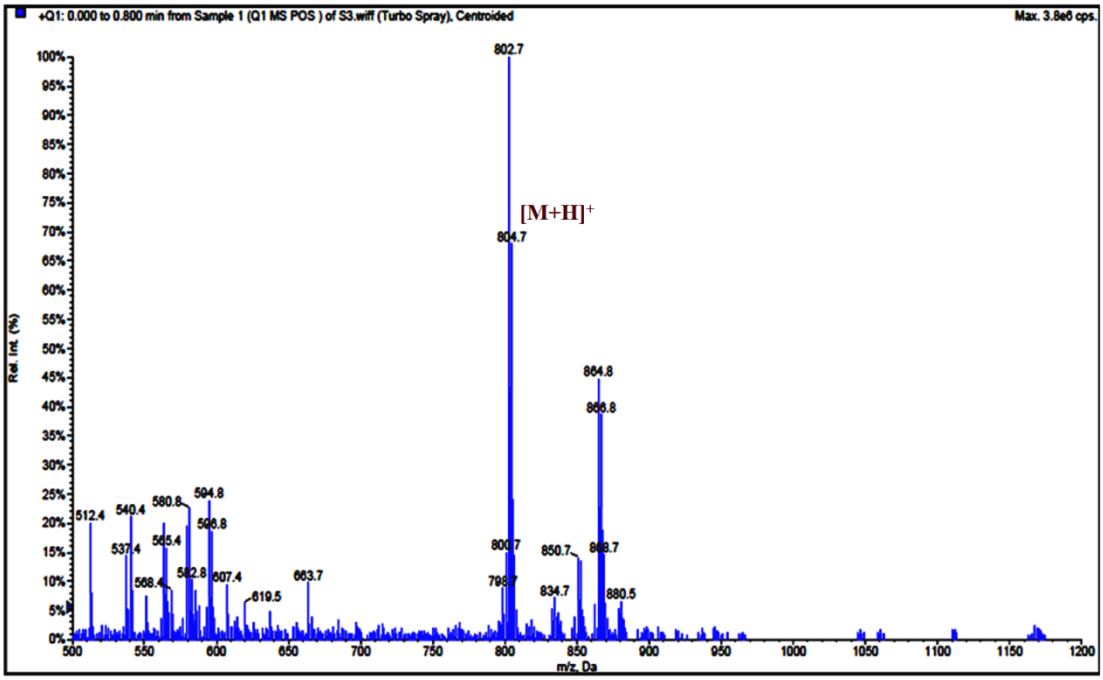

Figure S11. LC MS spectra of complex 8

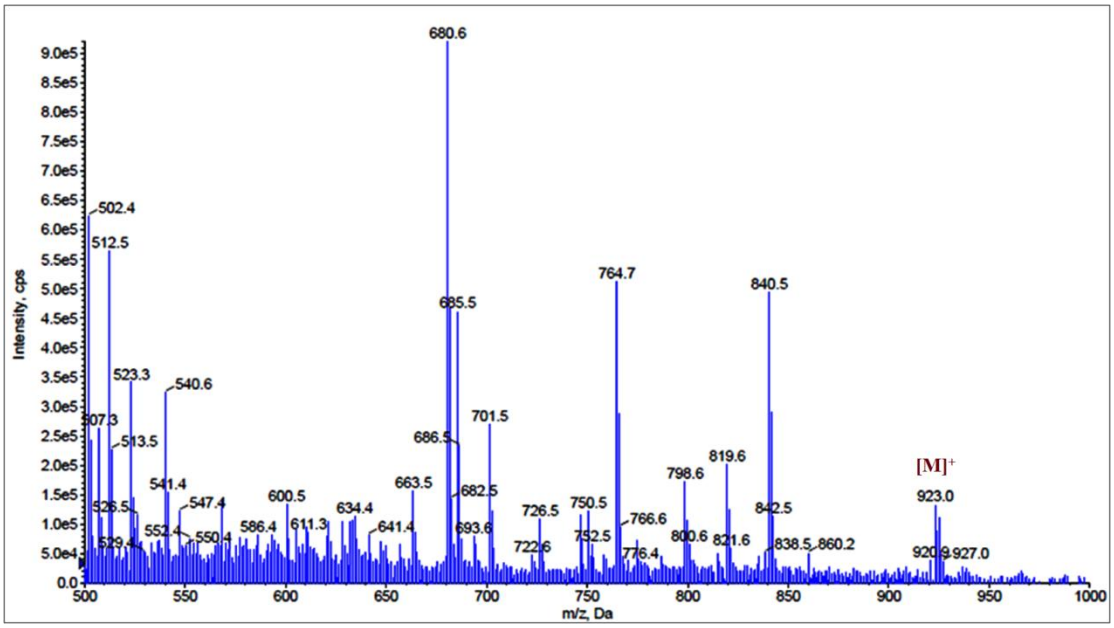

Figure S12. LC MS spectra of complex 9

2.6.3. NMR spectra

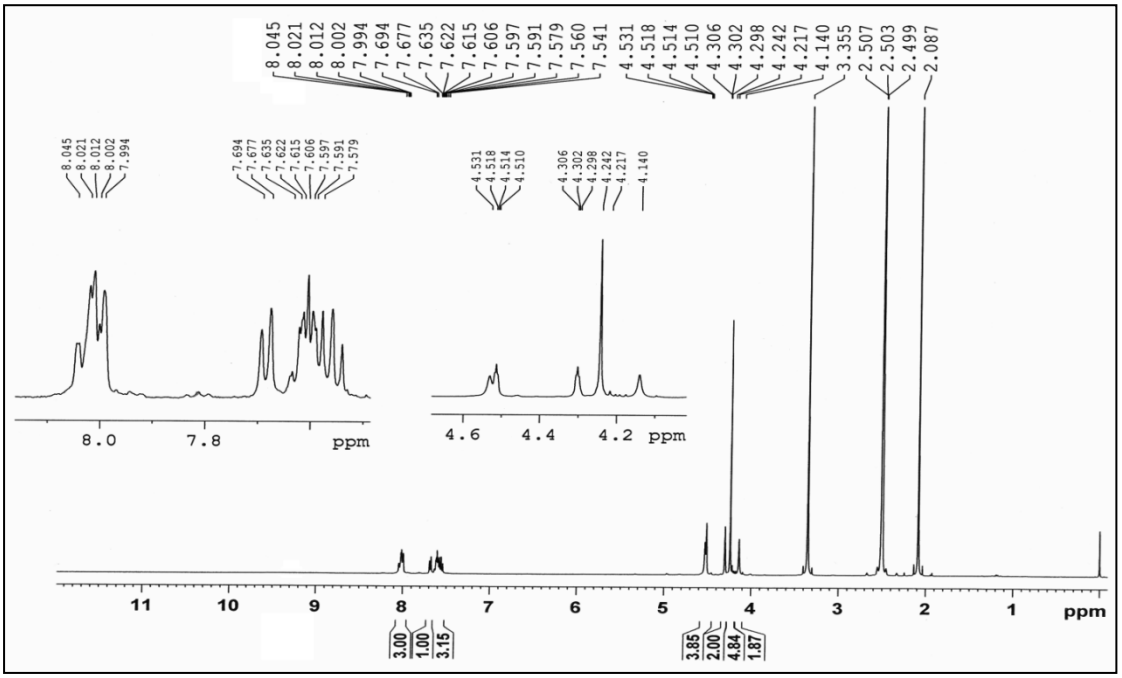

Figure S13. ^{1}H NMR spectrum of *N*-methyl-(1-naphthyl)-*N*-methyl ferrocenyl amine (L^1)

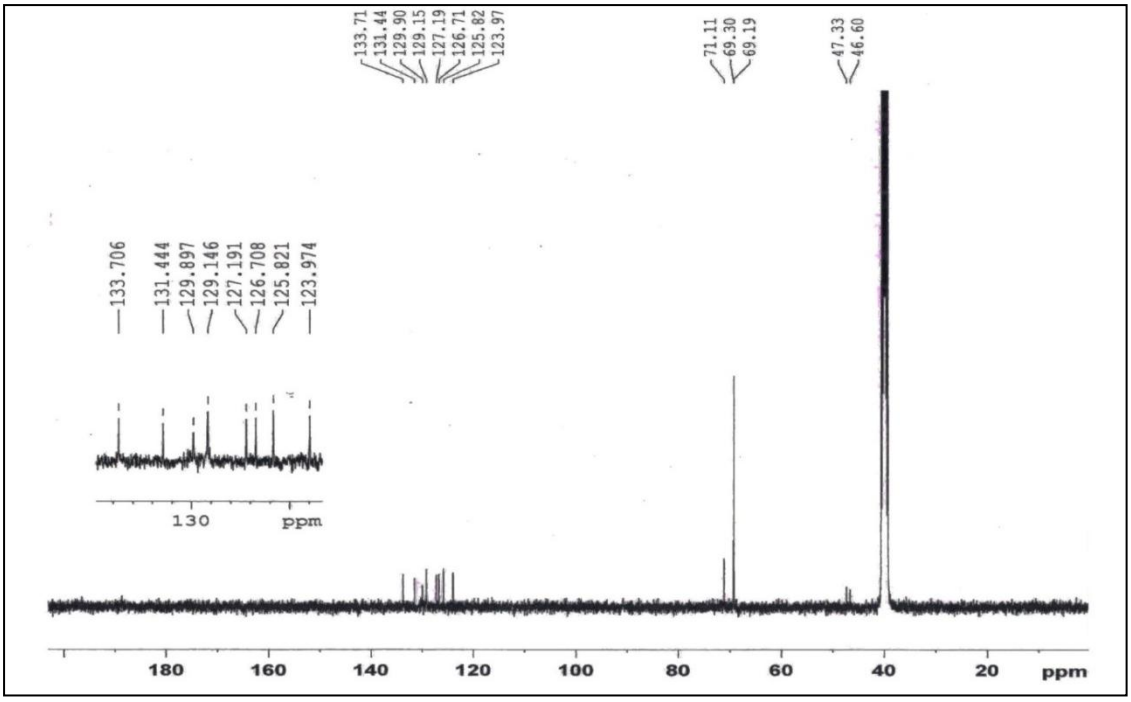

Figure S14. ^{13}C NMR spectrum of *N*-methyl-(1-naphthyl)-*N*-methyl ferrocenyl amine (L^1)

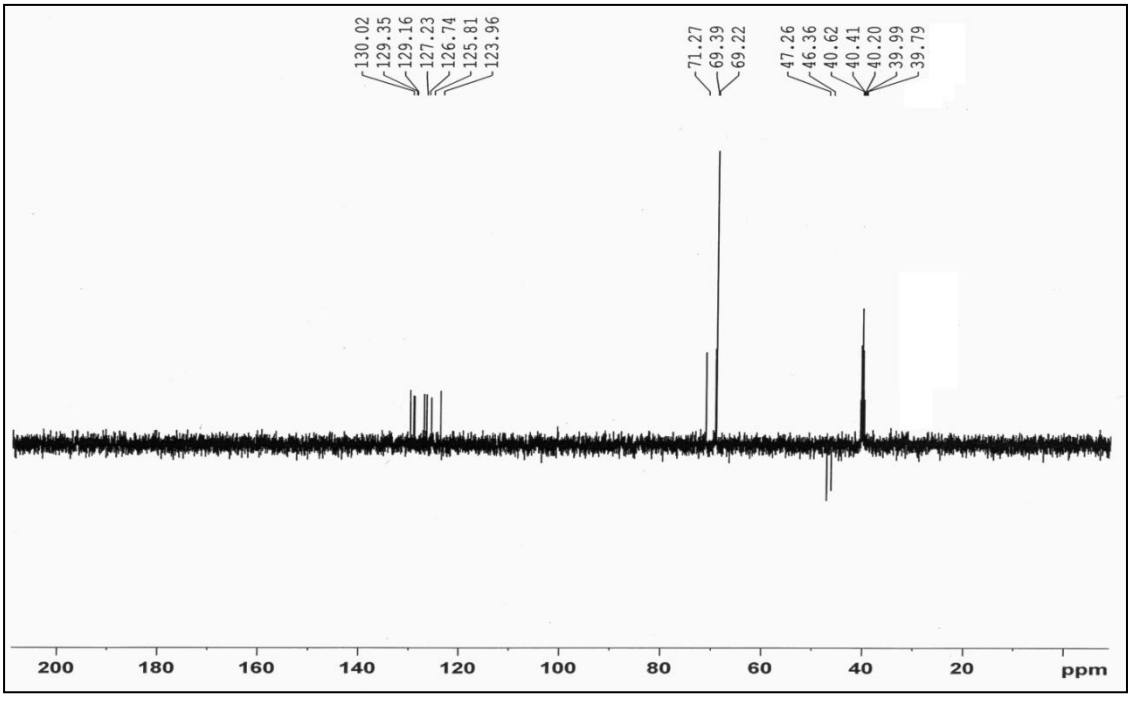

Figure S15. DEPT 135 NMR spectrum of *N*-methyl-(1-naphthyl)-*N*-methyl ferrocenyl amine (L^1)

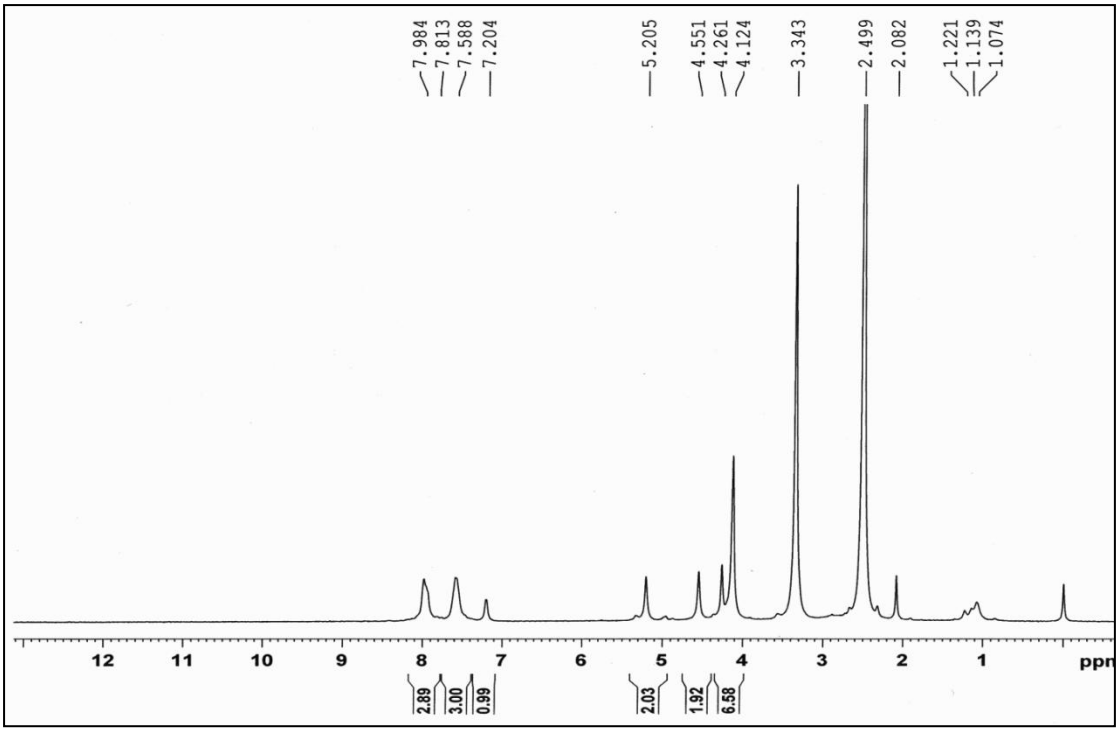

Figure S16. ^{1}H NMR spectrum of compound 4

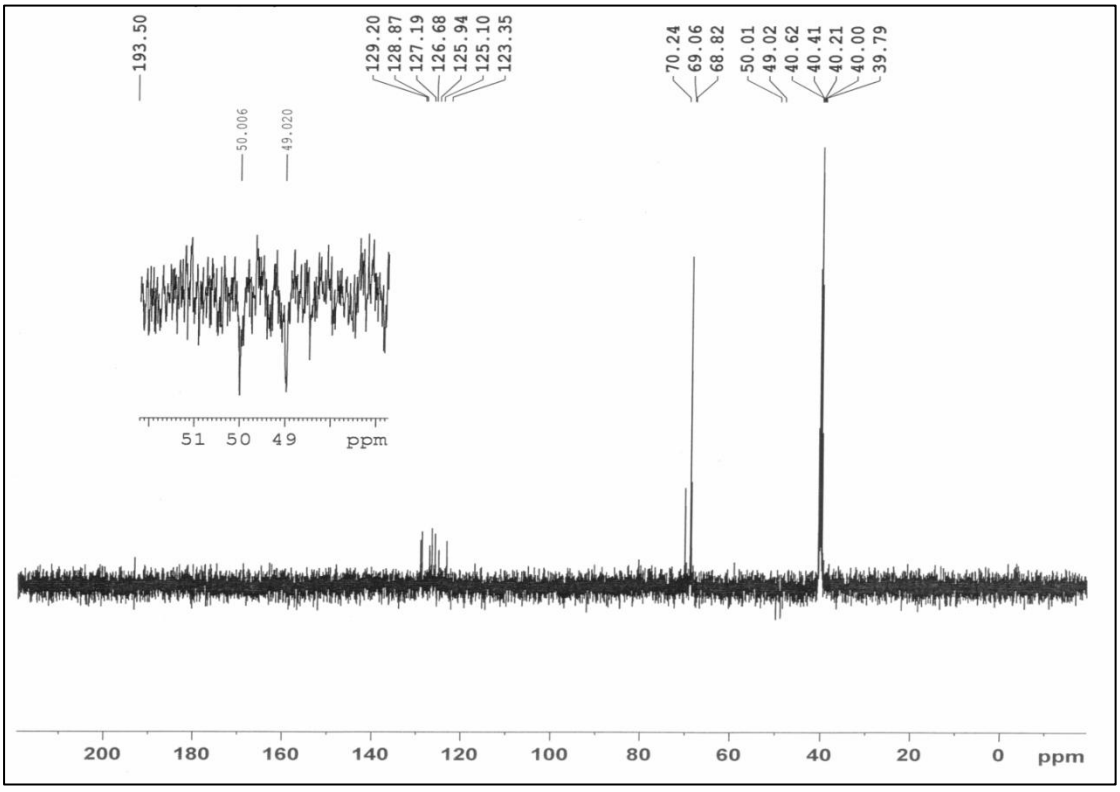

Figure S17. DEPT 135 NMR spectrum of compound 4

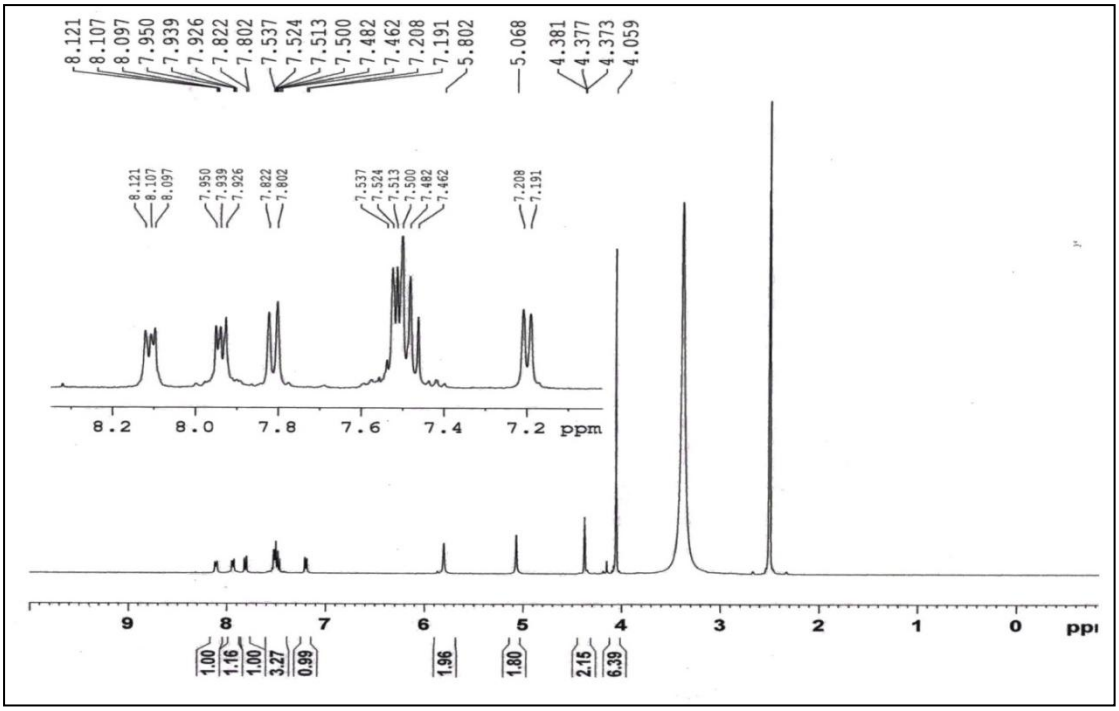

Figure S18. ^{1}H NMR spectrum of compound 9

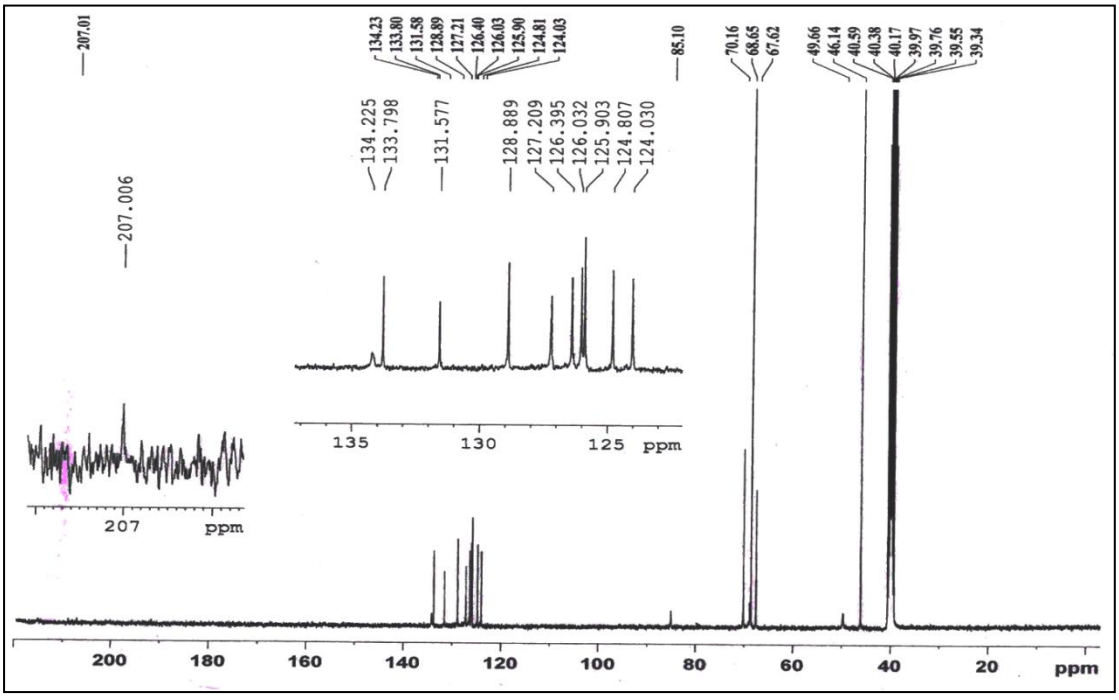

Figure S19. ^{13}C NMR spectrum of compound 9

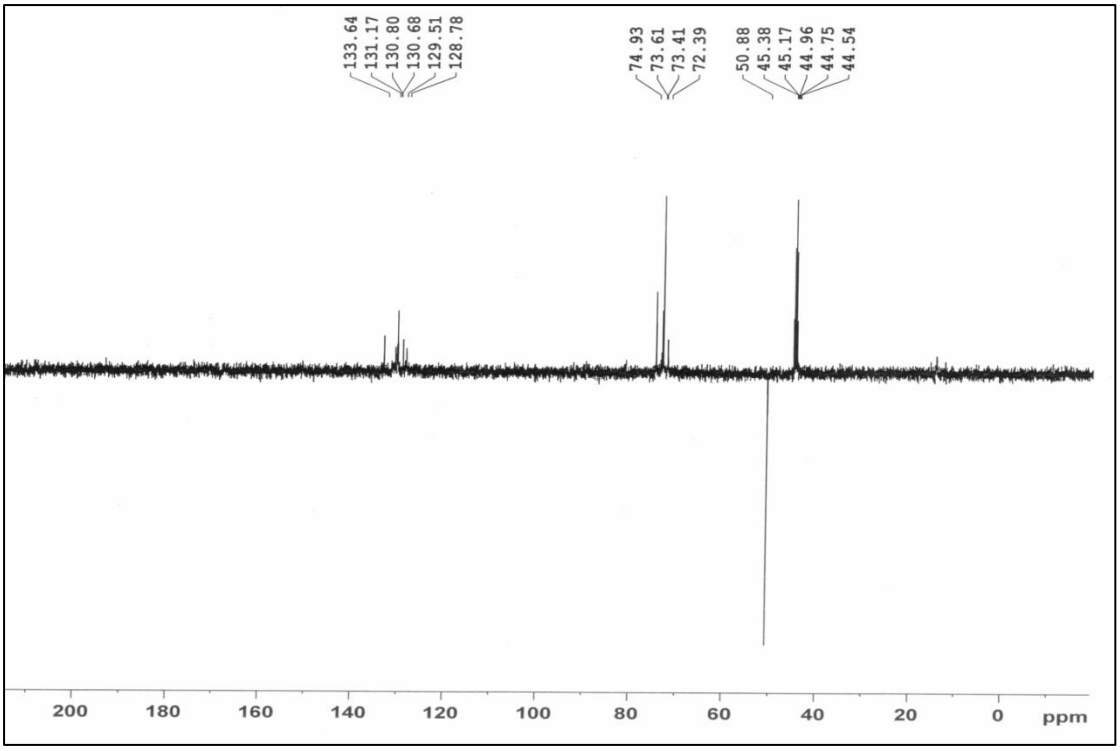

Figure S20. DEPT 135 NMR spectrum of compound 9

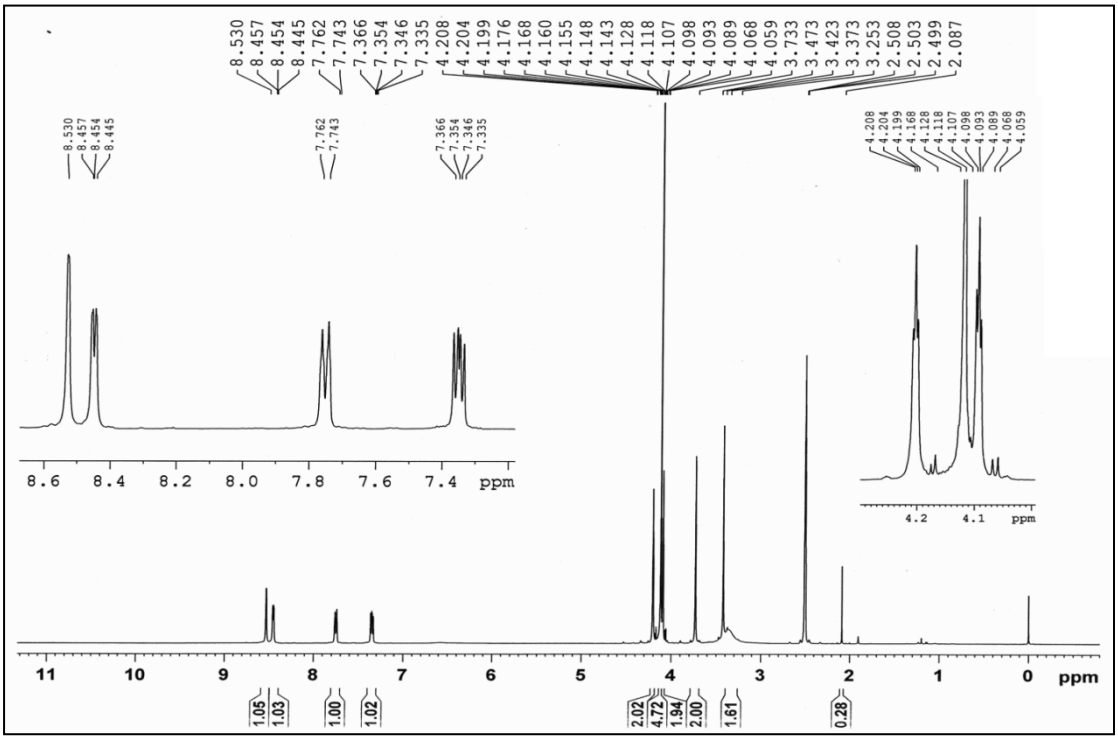

Figure S21. ^{1}H NMR spectrum of *N*-methyl-(3-pyridyl)-*N*-methylferrocenyl amine (L^2)

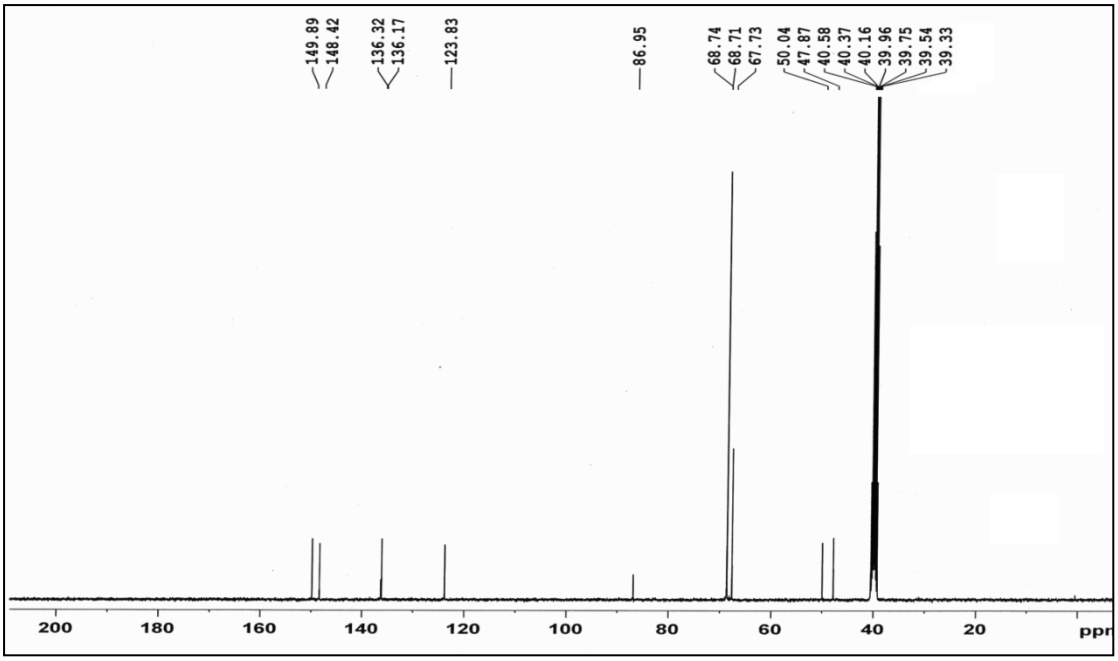

Figure S22. ^{13}C NMR spectrum of *N*-methyl-(3-pyridyl)-*N*-methylferrocenyl amine (L^2)

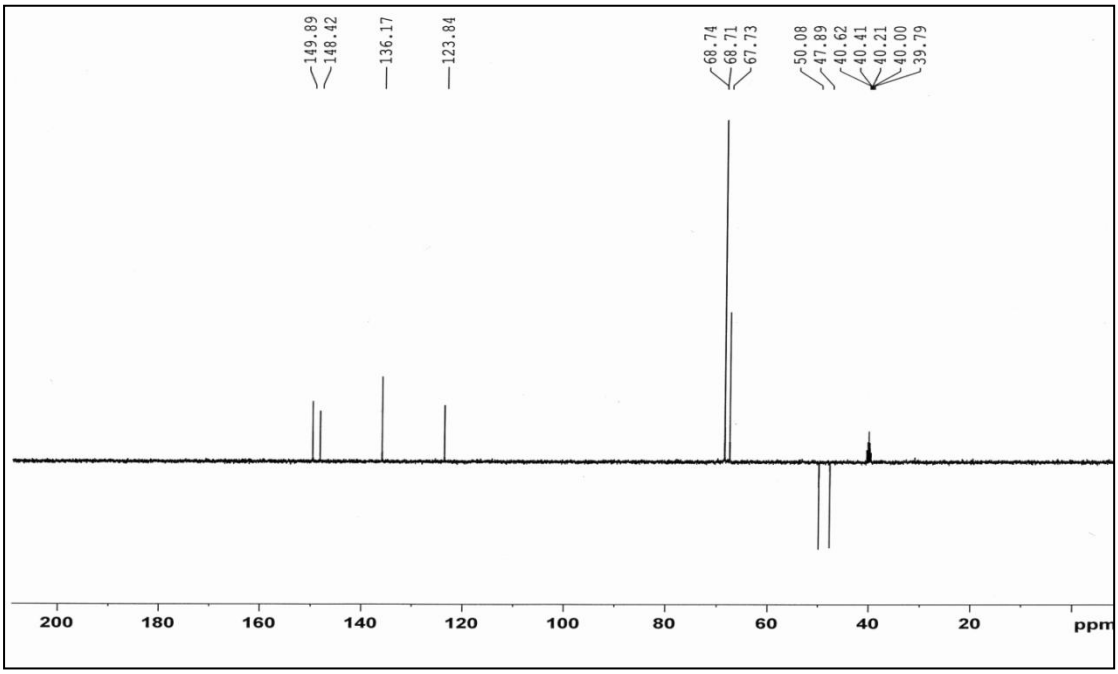

Figure S23. DEPT 135 NMR spectrum of *N*-methyl-(3-pyridyl)-*N*-methylferrocenyl amine (L^2)

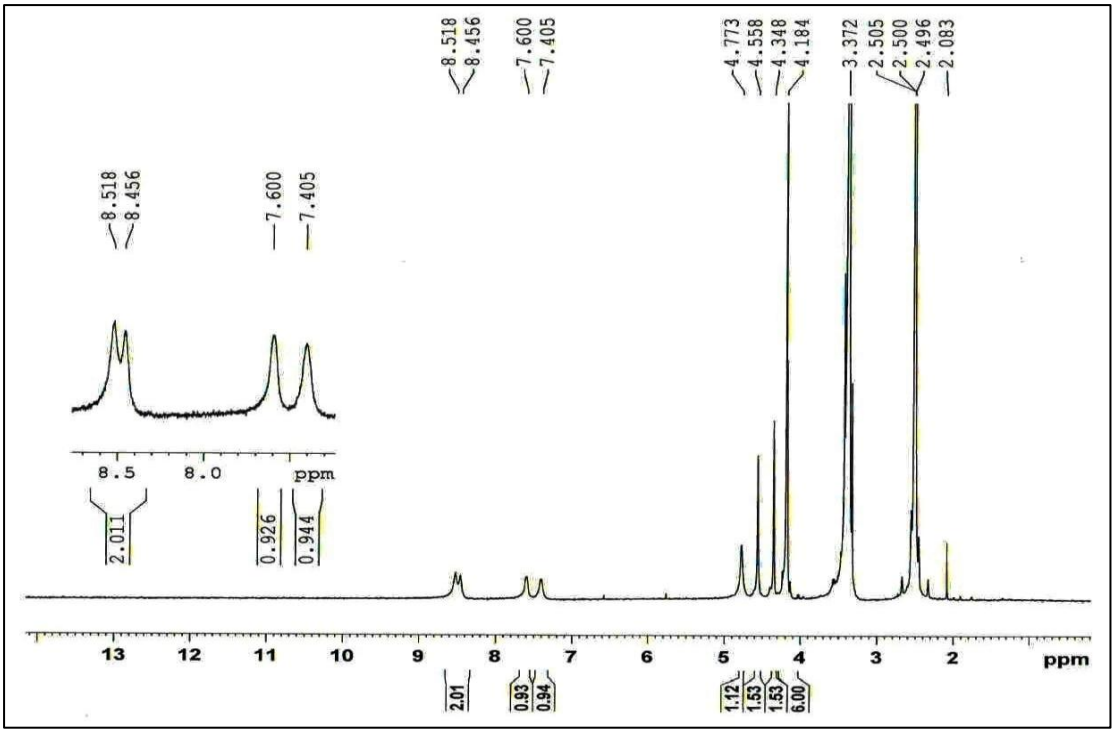

Figure S24. ^{1}H NMR spectrum of complex 5

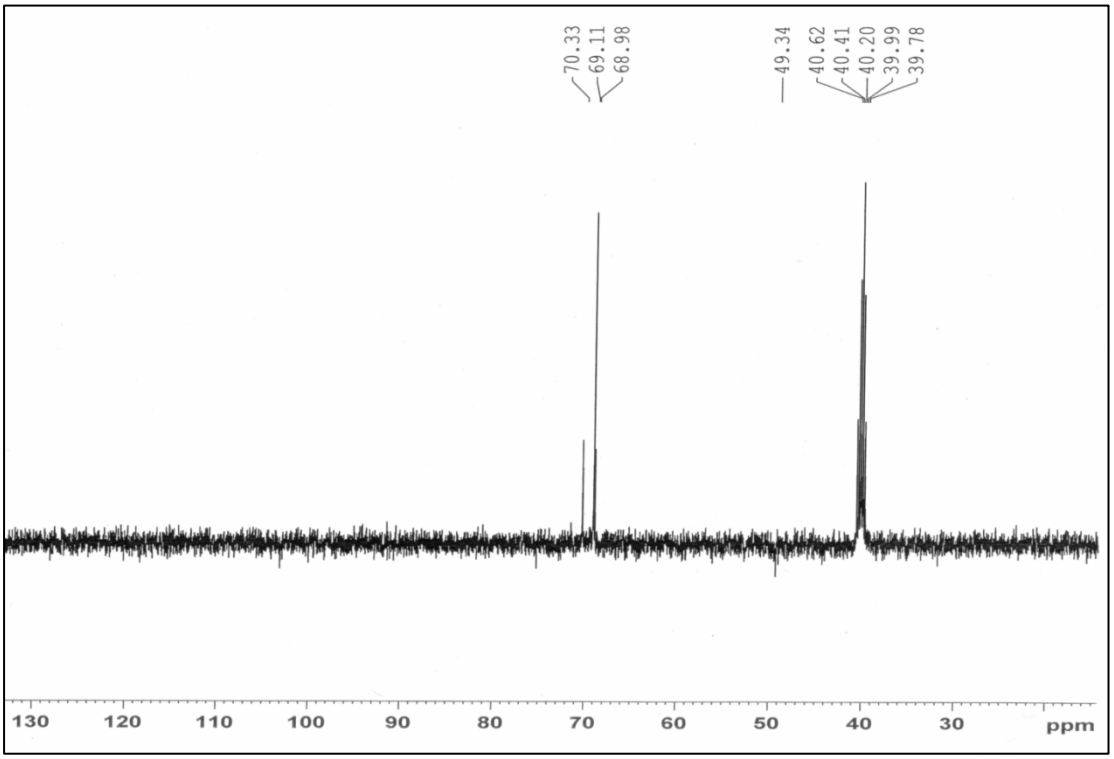

Figure S25. ^{13}C DEPT 135 NMR spectrum of complex 5

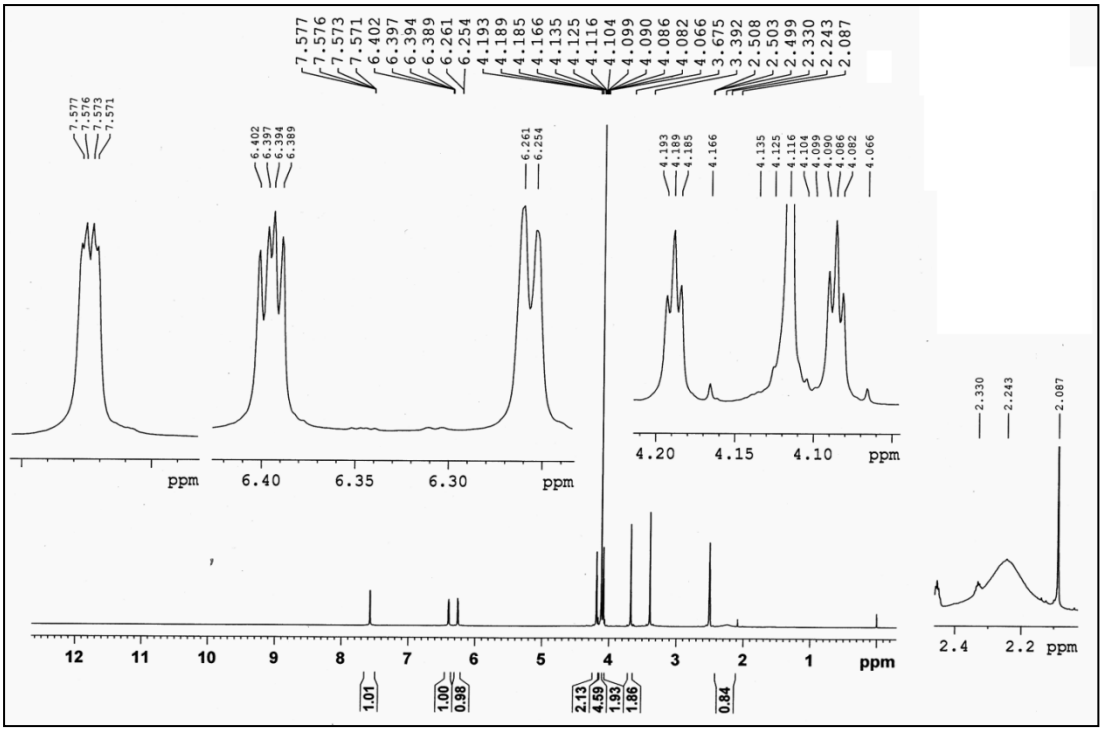

Figure S26. ^{1}H NMR spectrum of *N*-furfuryl-*N*-methylferrocenyl amine (L^3)

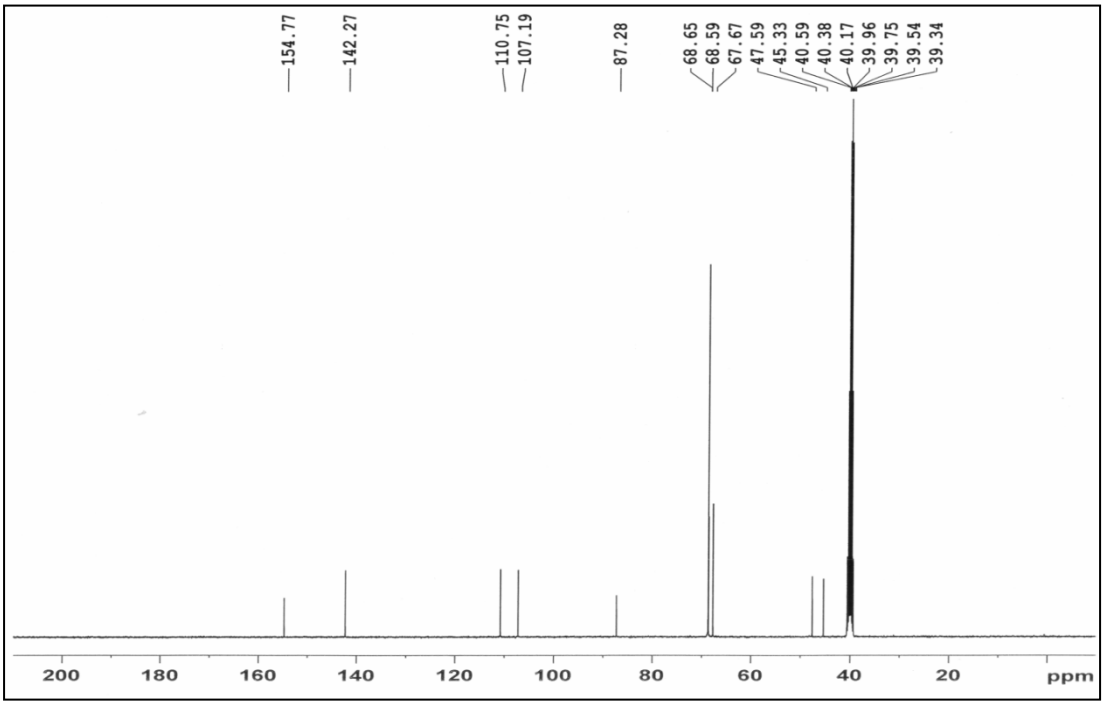

Figure S27. ^{13}C NMR spectrum of *N*-furfuryl-*N*-methylferrocenyl amine (L^3)

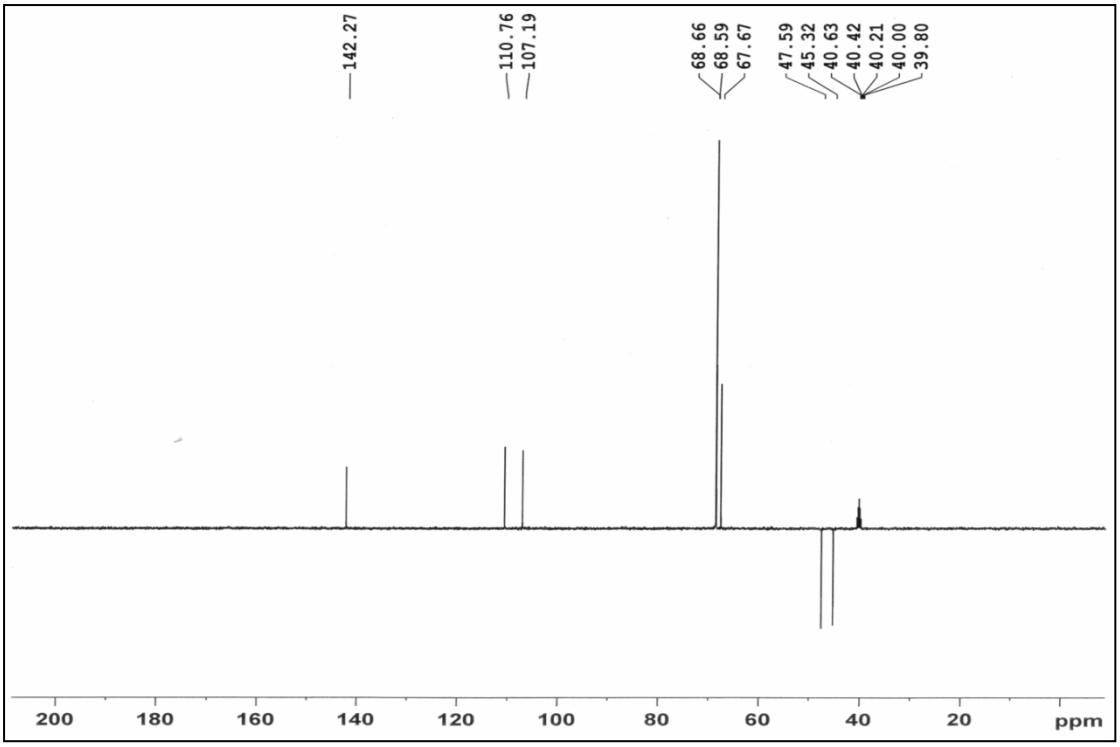

Figure S28. DEPT 135 NMR spectrum of *N*-furfuryl-*N*-methylferrocenyl amine (L^3)

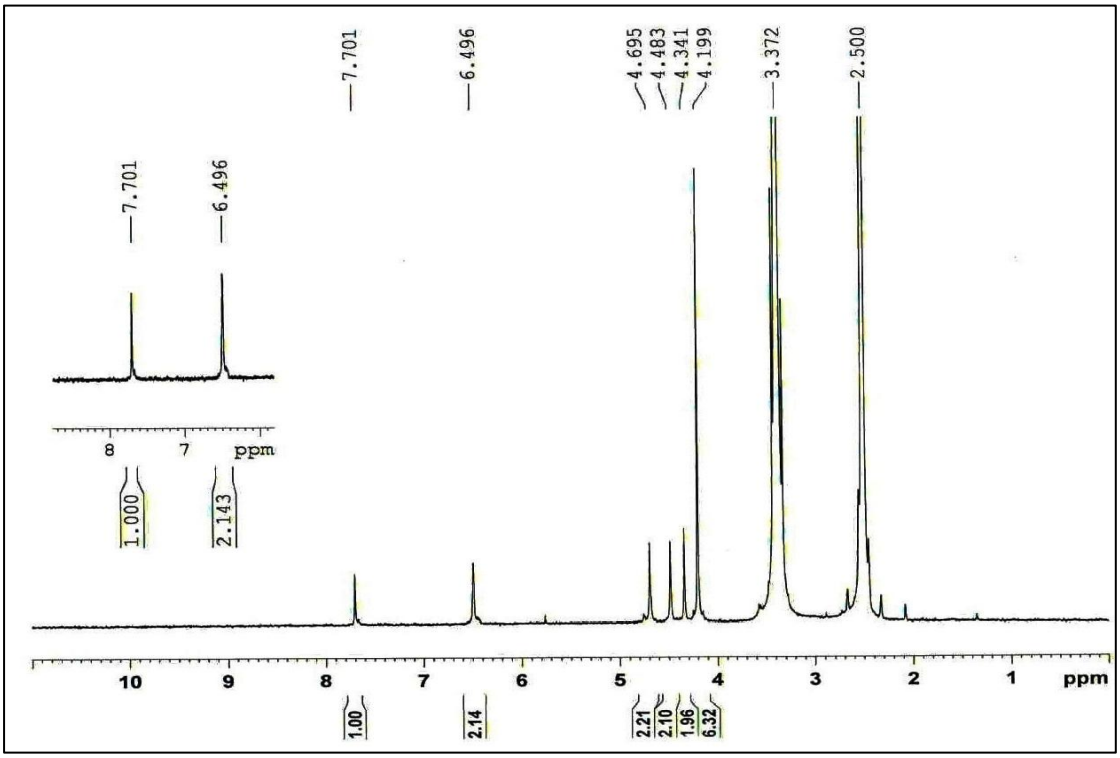

Figure S29. ^{1}H NMR spectrum of complex 6

2.6.4. Thermogravimetric Analysis

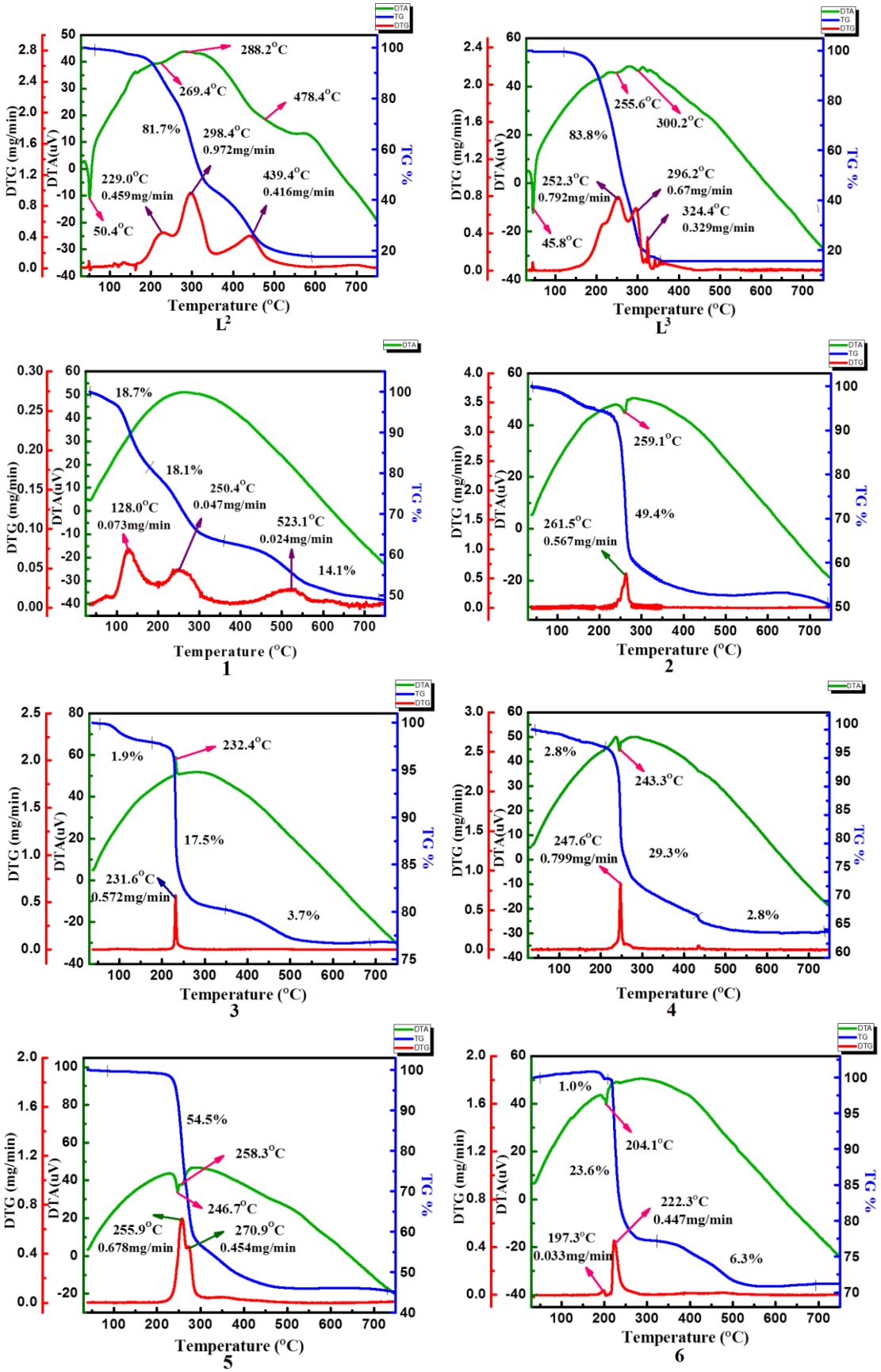

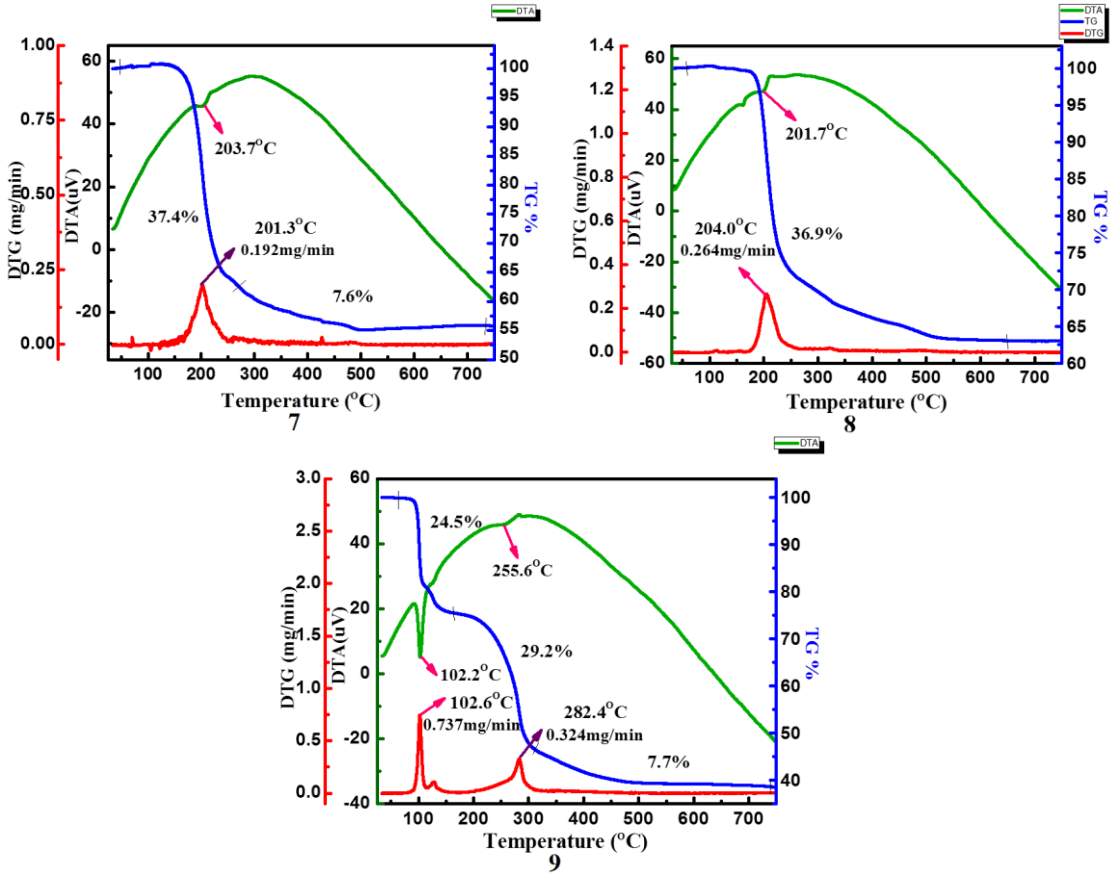

Figure S30. TG/DTA curves of the ligand precursor *N*-methyl-(3-pyridyl)-*N*-methylferrocenyl amine (L^2), *N*-furfuryl-*N*-methylferrocenyl amine (L^3) and new dithiocarbamato metal complexes **1-9**.